Geotech Geol Eng (2015) 33:1141–1166
DOI 10.1007/s10706-015-9892-6

ORIGINAL PAPER

Coupled Behavior of Cemented Paste Backfill at Early Ages

Alireza Ghirian · Mamadou Fall

Received: 11 December 2013 / Accepted: 12 May 2015 / Published online: 20 May 2015

Abstract Once cemented paste backfill (CPB) is poured into a mine stope, it is subjected to strong coupled thermal (T), hydraulic (H), mechanical (M) and chemical (C) processes. A laboratory investigation is performed to understand the THMC behavior of CPB at early ages. An experimental setup is developed to study the THMC behavior of CPB. The testing and monitoring are conducted in undrained conditions, with and without pressure application, and take into consideration two types of tailings (artificial and natural). The evolutions of the total pressure, pore pressure, suction, temperature and electrical conductivity are monitored for a period of 7 days. Also, the CPB samples are tested or analyzed with regards to their shear strength properties, hydraulic conductivity, thermal conductivity, and physical and microstructural characteristics at 1, 3 and 7 days. The obtained results show that the THMC properties of CPB are strongly coupled due to several mechanisms, such as curing stress, heat of hydration, self-desiccation and pore fluid chemistry. The results presented in this paper will provide a better understanding of the THMC behavior of CPB at early ages and thus contribute to the better designing of CPB structures.

A. Ghirian · M. Fall (✉)
Department of Civil Engineering, University of Ottawa, 161 Colonel By, Ottawa, ON K1N 6N5, Canada
e-mail: mfall@eng.uottawa.ca; mfall@uottawa.ca

Keywords Cemented paste backfill · Tailings · Coupled processes · THMC · Cement · Mine

1 Introduction

During ore rock extraction, mining operations produce huge quantities of tailings and waste rock (Ritcey 2005; Kesimal et al. 2005). The disposal of tailings on the surface can cause serious geoenvironmental problems (Yilmaz et al. 2003; Huynh et al. 2006; Ercikdi et al. 2009; Fall et al. 2010b; Mahlaba et al. 2011; Farkish and Fall 2013, Wu et al. 2013). Additionally, the creation of mined-out underground spaces (stopes) results in surface subsidence and mining workplace instability (Rankine et al. 2001; Li and Aubertin 2009). A common practice for rectifying this problem is to utilize the waste tailings in filling mine stopes with cemented paste backfill (CPB). CPB is a mixture of dewatered mill tailings and binding agent, with added water to achieve the required consistency for transporting the CPB to the mine stope (Fall et al. 2005, 2010a; Kesimal et al. 2005; Huang et al. 2011; Cihangir et al. 2012).

Once placed, the CPB structure is subjected to strong coupled thermal (T), hydraulic (H), mechanical (M) and chemical (C) (THMC) processes or factors (Fig. 1). An understanding of the interplays between these different processes demands a comprehensive study of the fully coupled THMC behavior which is crucial for a reliable and cost-effective design of the

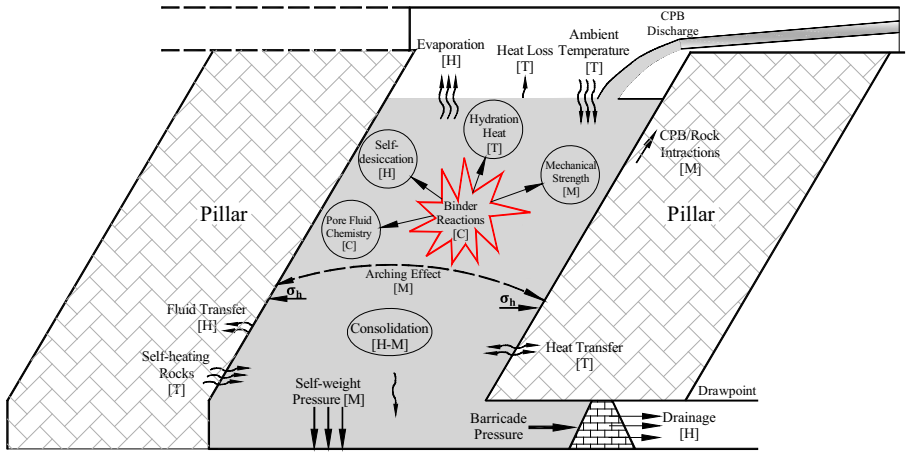

Fig. 1 Schematic diagram of different THMC coupled processes in a backfill structure (static condition)

backfill structure. Although there have been many studies that investigate each specific factor (e.g., Hassani and Archibald 1998; Yilmaz et al. 2004; Kesimal et al. 2005; Klein and Simon 2006; Ercikdi et al. 2010; Orejarena and Fall 2010, 2011; Nasir and Fall 2009, 2010; Cihangir et al. 2012; Wu et al. 2012; Yin et al. 2012), to date, no comprehensive study has been conducted to address the coupled THMC behavior of CPB cured under stresses comparable to those generated by the CPB weight.

CPB filled stopes must have sufficient mechanical stability (usually evaluated by the strength of the CPB) in order to remain stable or self-supporting during the recovery of the adjacent stopes (Fall et al. 2007). A common practice that is used to assess the backfill strength is to conduct unconfined compressive strength (UCS) tests on small laboratory samples (20×10 cm or 10×5 cm) of CPB cured in conventional plastic molds at atmospheric pressure and temperature conditions. The obtained information is limited since the influence of various important factors, such as self-weight pressure, filling rate, drainage condition, and heat of cement hydration, cannot be included in the strength assessment. This can result in a conservative design approach, which in turn, increases the cost in terms of cement consumption, barricade construction and stope cycle times (e.g., le Roux et al. 2005; Thompson et al. 2009). Furthermore, backfill strength gain depends on the suction development as a result of self-desiccation and/or drainage, or sometimes desaturation (drying out) (Helinski et al. 2006; Abdul-Hussain and Fall 2011). Suction can increase the effective stress, which in turn, decreases the vertical stress in the backfill as well as reduces the horizontal stress on a barricade as observed through the in situ instrumentation of some mine stopes (e.g., Thompson et al. 2009). Only a few studies have been experimentally conducted to study the effect of self-weight pressure (e.g., Belem et al. 2002; Yilmaz et al. 2009, 2014), suction development as a result of self-desiccation (e.g., Helinski 2007); and heat of hydration (e.g., Fall and Samb 2009; Fall et al. 2010a) on backfill strength assessment. However, no studies have been performed to investigate the coupled effect of the THMC processes on the strength of CPB cured under different stresses. Furthermore, there are no studies on the THMC behavior of CPB cured under stress and the effect of these THMC processes on other relevant design factors of CPB, such as thermal (e.g., thermal conductivity, heat of hydration), hydraulic (e.g., pore water pressure (PWP), suction, permeability), chemical (e.g., evolution of pore water chemistry, binder hydration), mechanical (e.g., deformation), and physical (microstructure, density) factors (see Fig. 1).

Ghirian and Fall (2013, 2014) investigated the THMC behavior of CPB by means of a high column experiment to understand the governing coupled processes in an almost stress free state. Since the tops of the columns were open to the atmosphere, they could also investigate the effect of evaporation and associated surface shrinkage on the hydro-mechanical behavior of CPB. However, the effect of mechanical load as a result of self-weight pressure on THMC

behavior was not considered in their studies. In the current study, a pressure cell apparatus is developed to investigate the THMC coupled processes in CPB. The new setup grants privileges to simulate curing conditions relatively close to underground mine stope conditions at a laboratory scale with controlled rate of loading (i.e., stope filling). It also enables to cure samples that are relatively large in size for testing purposes.

The objective of the study was to investigate the early age THMC behavior of CPB cured under various stresses. The main coupled interactions between different processes were determined and the effect of the curing stress on each individual factor was studied. Furthermore, by conducting THMC studies on two types of tailings (natural and artificial), the effect of tailings type and its chemical composition on the THMC performance of CPB material was investigated.

2 Materials and Methods

2.1 Materials

The materials used for the CPB preparation include binder, tailings, and water.

2.1.1 Tailings

Two types of tailings, which include natural zinc tailings (ZnT) and artificial silica tailings (ST), were used to prepare the fresh CPB. The natural tailings used in this study are fine-grained tailings from a mine located north of Canada, one of the Canada's largest zinc mines. The artificial tailings contain ground silica with 99.8 % SiO_2. The main benefit of the use of non-reactive ST is to accurately control the chemical and mineralogical compositions. Natural tailings may contain several reactive chemical elements and often, sulphide minerals, which can interact with cement and thus, affect the interpretation of the results and/or introduce significant uncertainties in the results obtained (Nasir and Fall 2008). The mineral compositions of both types of tailings used for the CPB preparation were obtained from an x-ray diffraction (XRD) analysis, and presented in Table 1. More than 50 % of the silica particles are smaller than 25 μm (D_{50}) and 10 % are smaller than 2 μm (D_{10}). According to the Unified Soil Classification System (USCS), both the ST and ZnT are non-plastic silt (ML), as are most of the tailings produced by hard rock mines (Orejarena and Fall 2008, 2011). The grain size distribution of the ST and the ZnT are presented in Fig. 2, which are close to the average of nine Canadian hard-rock metal mine tailings. The physical properties of both types of tailings are tabulated in Table 2.

2.1.2 Cement and Water

The most popular cement used in backfill preparation is ordinary Portland cement type I (PCI) which is used in this study. The characteristics of the PCI are presented in Table 3. Tap water was used to mix the cement and tailings.

2.2 Specimen Preparation and Mix Proportions

The CPB mix design included PCI (4.5 % wt), and a water to cement ratio (*w*/*c*) equal to 7.6. The tailings material, cement and water were mixed and homogenized in a food mixer for about 7 min. In all of the mixes, the *w*/*c* ratio and cement proportions were kept constant. The slump or the consistency of the paste mixtures was measured by a slump test in accordance with ASTM C143. The slump values for the CPB prepared with ST and ZnT were about 18 cm and 22 cm, respectively, which belong to the most frequent slump values used in CPB preparation and transportation into mine stopes. The average values of the initial physical characteristics of the fresh CPB made of ST or ZnT are presented in Table 4. The CPB mixtures were mixed and then loaded into a pressure cell apparatus. In total, three test series were conducted: (i) C-ST test series (or control tests) were conducted on samples prepared with ST and cured without applying any vertical pressure, and the results were considered as the reference values in order to compare the effect of pressure application on THMC evolution; (ii) CUS-ST test series, and (iii) CUS-ZnT test series, which were conducted under curing stress, and the CPB specimens were prepared with ST or ZnT, respectively.

2.3 Developed Pressure Cell Apparatus

The main purpose of the developed experimental setup is to simulate the mine stope filling sequence and overburden pressure (self-weight stress) during the

Table 1 Mineral composition of the tailings used

Element/tailings	Quartz	Dolomite	Chlorite	Magnetite	Pyrite	Talc	Magnesite	Actinolite	Pyrrhotite	Spinel	Others
ZnT (wt %)	11.9	5.7	18.2	11.4	15.4	16.4	7.6	3.2	3.1	3.2	3.9
ST (wt %)	99.8	–	–	–	–	–	–	–	–	–	–

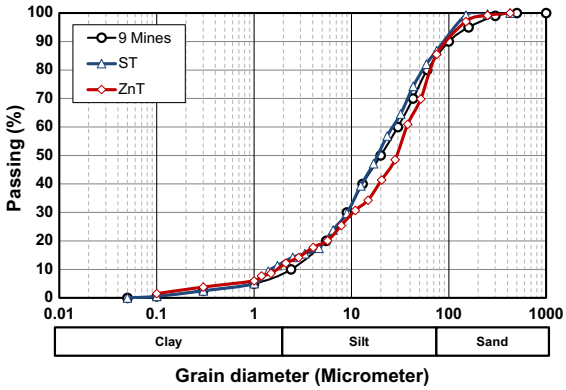

Fig. 2 Grain size distribution of studied tailings compared with the average of 9 Canadian hard-rock metal mine tailings

Table 4 Mean values of initial physical characteristics of CPB prepared with ST and ZnT

Properties	ST	ZnT
Void ratio, e	1.15	1.92
Specific gravity, Gs	2.71	3.34
Degree of saturation, Sr (%)	100	100
Solid content by mass, C_W (%)	74.4	74.8
Solid content by volume, C_V (%)	39.7	33.1
Water content, ω (%)	33.7	35.4
Water to solid ratio (w/s)	0.34	0.34
Slump (cm)	18	22
W/C	7.6	7.6

curing of CPB. Furthermore, the setup provides a facility that monitors the evolution of the key THMC factors, such as the evolution of pore water pressure, suction, binder hydration, deformation and temperature of the CPB with time for a mix design. Furthermore, the setup allows the sampling of CPB specimens cured under the above-mentioned mine stope conditions for the purpose of conducting the required geotechnical, microstructural and chemical testing, such as uniaxial compressive strength (UCS), shear strength, saturated hydraulic conductivity and thermal property tests, and microstructural and chemical analyses to investigate the THMC properties of the CPB material. Figure 4 presents a schematic diagram of the developed experimental setup (pressure cell apparatus to measure THMC). A Perspex (acrylic plastic) cylinder with the diameter of 101.6 mm (4 in.) and height of 304.8 mm (12 in.) was employed as the main framework to hold the samples at a one-dimensional vertical pressure. An axial piston was mounted on the upper portion of the cylinder to apply the required pressure up to 600 kPa, which is equal to approximately 35 m on a mine stope. Compressed air pressure was used as the driving force on the piston. The pressure increment was controlled

Table 2 Physical properties of the tailings used

Tailings	G_s	D_{10} (μm)	D_{30} (μm)	D_{50} (μm)	D_{60} (μm)	C_u	C_c
ST	2.70	1.9	9.0	22.5	31.5	16.6	1.3
ZnT	3.34	1.6	10.9	29.9	37.8	23.6	2.0

Table 3 Characteristics of Portland cement type I

Type of binder	MgO (%)	CaO (%)	SiO_2 (%)	Al_2O_3 (%)	Fe_2O_3 (%)	SO_3 (%)	Relative density	Specific surface (m^2/g)
PCI	2.65	62.82	18.03	4.53	2.70	3.82	3.10	1.30

by a regulator and pressure gauge. A top and a bottom plate with three tie rods were used to support the Perspex mold against leakage and internal pressure. Only 200 mm of the cylinder was filled with CPB and the remaining space served as an air chamber to apply pressure on the piston. In all of the experiments, the length-to-diameter ratio of the CPB specimens was kept in the order of two.

In total, five cells were engineered and manufactured, including one cell for instrumentation and four cells for curing CPB samples at different curing times (1, 3 and 7 days). Studies have shown that undrained backfill exhibits weaker mechanical properties than drained backfill (e.g., le Roux et al. 2005). Therefore, in consideration of this case scenario, an undrained condition was adopted for all of the experiments. This represents a conservative approach with regards to the mechanical stability of field CPB structure.

In underground mine stopes, cement hydration is usually the main source of temperature increase within the backfill structure (Fall et al. 2010a). Thermal factors, such as heat of hydration, can accelerate the rate of the binder hydration, and thus the rate of the strength gain in CPB materials (Fall et al. 2010a). This can be considered as the coupled effect of temperature and chemical reactions (thermo-chemical coupling). Therefore, in this study, all of the cells were covered with a 100 mm heat insulation glass wool blanket after loading the CPB. This enables to restrict heat loss from the CPB as well as maintain the heat of hydration during the curing time to investigate its effect on the THMC behavior of the CPB.

2.3.1 Applied Vertical Pressure

In this study, an average filling rate equal to 0.131 m/h is chosen to find the corresponding increments of applied pressure and equivalent mine backfill height. Figure 3 presents the pressure application scheme that simulates mine stope backfilling over a period of 7 days. The applied vertical pressure due to stope filling and corresponding equivalent backfill height ($h = \sigma_v/\gamma$) were calculated based on the CPB bulk unit weight which is equal to 17.2 kN/m^3. It should be noted that the arching effect is not included in this study due to the mechanism of the pressure cell (one-dimensional vertical pressure). The pressure was gradually increased every 3 h for the first 12 h and up to 150 kPa in order to simulate a more realistic self-weight pressure on the specimen. Then, the pressure was increased every 24 h up to 600 kPa, which is equivalent to 34.9 m or an average filling rate of 0.31 m/h.

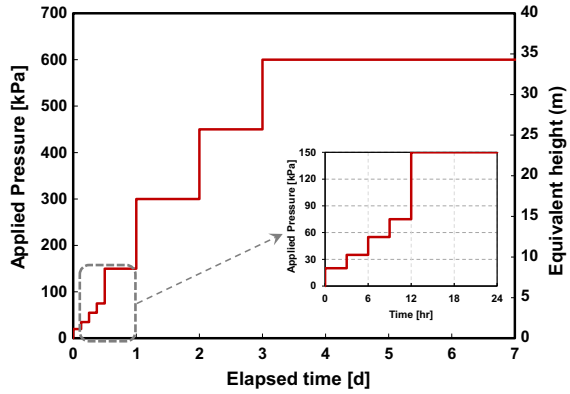

Fig. 3 Pressure application scheme which simulates a 30 m mine stope and average filling rate of 0.31 m/h

2.3.2 Pressure Cell Instrumentation and Monitoring

One of the five cells was equipped with various sensors, including a pressure transducer, a vibrating wire piezometer, a suction meter and an electrical conductivity (EC) sensor located at the lower portion of the cell. A linear variable differential transformer (LVDT) was also attached to the piston rod at the top of the cell to record any deformations as a result of applied pressure and/or binder hydration. The locations of all the sensors are schematically illustrated in Fig. 4. The THMC evolution of the CPB was continuously monitored in terms of the heat of cement hydration, total pressure, pore water pressure (PWP) response, suction evolution, electrical conductivity evolution and deformation for a period of 7 days. All of the sensors were connected to the appropriate data loggers to record the data with time. The monitoring of suction development with time was conducted by using a dielectric water potential sensor, model MPS-2. This sensor is capable of measuring suction between −10 and −500 kPa. The pressure transducer and suction meter were installed 40 mm above the cell bottom in order to monitor the total pressure and suction evolution with time. A vibrating wire piezometer was employed to monitor the consequences of sequential pressure application on the pore pressure evolution. For this purpose, a calibrated VW2100 standard vibrating wire piezometer with a 1 MPa pressure range

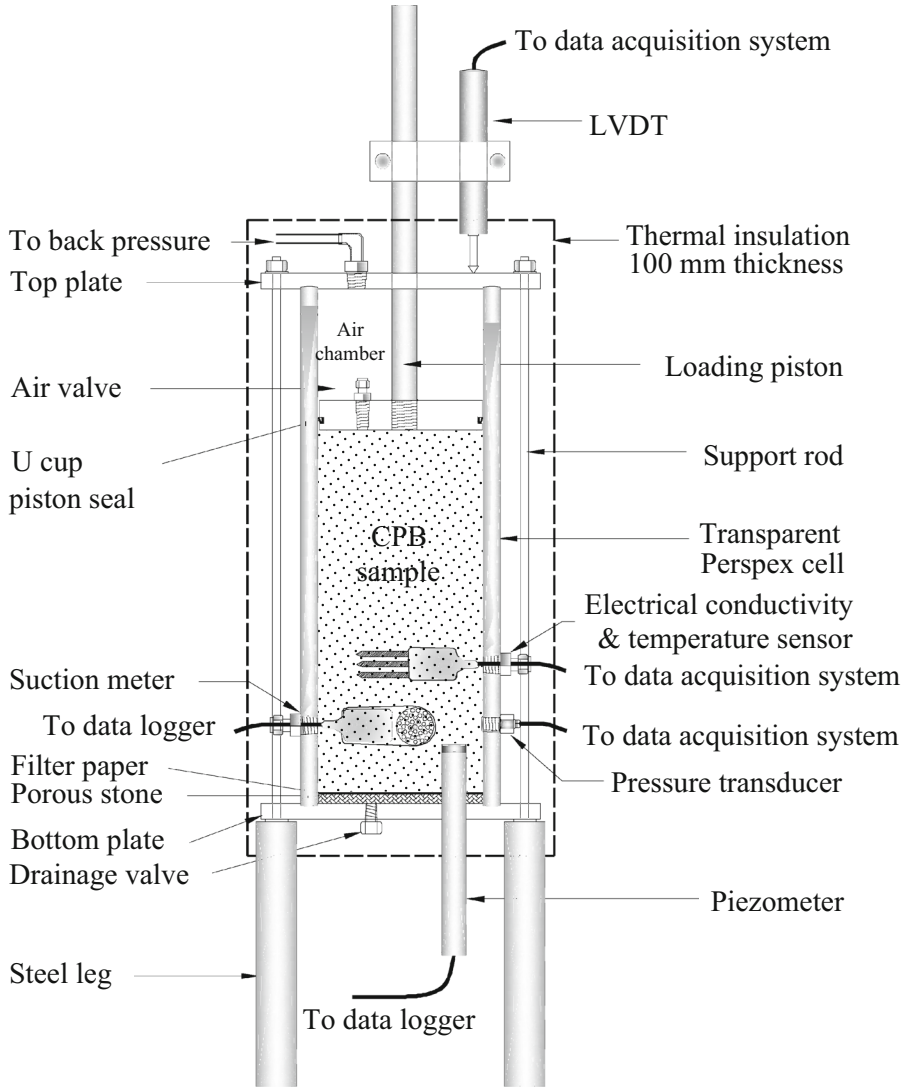

Fig. 4 Schematic diagram of the developed experimental set-up and arrangement of sensors

and ±0.1 % accuracy equipped with a standard air entry value ceramic disk was used. The tip of sensor was installed 30 mm above the bottom of the cell. The piezometer was equipped with a thermistor to measure the temperature as well. The ECH2O-5TE capacitance sensor was installed in the cell to measure the electrical conductivity with an accuracy of about ±10 %. EC is the ability of a material to conduct electricity. The sensor helped to monitor the setting time and rate of chemical reactions with time.

2.4 Experimental Test Program

In addition to the monitoring program described above, comprehensive laboratory tests were performed on the CPB samples cured at different ages to understand the THMC properties of the CPB material, as outlined in Table 5. All of the CPB samples were tested in terms of their thermal (i.e., thermal conductivity), hydraulic (i.e., saturated hydraulic conductivity), mechanical (UCS and shear strength parameters) and chemical properties (pore fluid chemistry). In addition, the physical properties and microstructure were evaluated (i.e., by mercury intrusion porosimetry (MIP) and scanning electron microscopy (SEM)) to understand the evolution of the index properties and pore structure of the CPB at early ages. The gravimetric water content (ω %) and bulk density (γ) of the samples were determined in accordance with ASTM D2216-10 and D7263-09,

Table 5 Summary of laboratory experimental testing and monitoring program

Test types	Mechanical (M)	Hydraulic (H)	Thermal (T)	Chemical (C)	Physical–Microstructural
Testing/analysis	UCS, shear strength, modulus of elasticity	Hydraulic conductivity	Thermal conductivity	Pore fluid chemistry	Porosity, density, moisture; by using SEM/MIP
Monitoring	Settlement	Pore pressure, suction	Heat of hydration	Electrical conductivity	–

respectively. Then, the void ratio (e) and porosity (n) were calculated at various curing times. The obtained test results are presented in the coming sections.

2.4.1 Mechanical Tests

Unconfined compression tests were performed on the CPB specimens at 1, 3 and 7 days of curing. A minimum of two samples (to ensure the repeatability of the results) were tested at each curing age in accordance with a standard test, ASTM C39, by means of a computer-controlled mechanical press. The compression tests were carried out at a constant deformation rate of 0.8 mm/min. Direct shear tests were carried out to determine the shear strength behavior and parameters (internal frictional angle and cohesion) of the CPB samples. This test is efficient and fast enough to conduct the tests at specific curing times. The test was performed in accordance with ASTM D3080-04 at a controlled strain rate of 1.0 mm/min. A minimum of four specimens were tested with different normal loads of 50, 100, 150 and 200 kPa to determine the failure envelopes.

2.4.2 Hydraulic Conductivity Tests

Saturated hydraulic conductivity tests were performed by using a TRI-FLEX II on the CPB specimens at each specific curing time. The flexible wall technique was used to determine the saturated hydraulic conductivity of the CPB. The procedure for this method is described in ASTM D5084 and was conducted in the constant head mode equal to 10 kPa. All of the samples were backpressure saturated. The saturation was also verified by determining the degree of the saturation of the samples at the completion of the hydraulic conductivity tests. The samples showed on average, final degrees of saturation that are higher than 99 %. Two samples were tested and at least three readings were done, and the average value was the saturated hydraulic conductivity of the sample tested.

2.4.3 Thermal Conductivity Tests

A KD_2 thermal property analyzer was utilized to measure the thermal conductivity of the CPB at different ages. This device computes the values of thermal conductivity by monitoring the dissipation in heat from a line source given a known voltage with ±5–10 % accuracy. To measure the thermal conductivity, first, a pilot hole with a diameter of 2.80 mm was drilled and then a thermal probe was inserted into the hole. To maximize the contact between the needle probe and the hole sidewall, a silver polysynthetic compound with high thermal conductivity ($k = 8$ w/m.k) was used. Each test was performed at least three times to verify the repeatability of the results.

2.4.4 Analysis of the Pore Fluid Chemistry

A pore fluid chemistry analysis was performed to understand the evolution of the pore fluid chemical composition of the CPB samples with time. In total, six samples prepared with ST and ZnT were tested at 1, 3 and 7 days. Pore fluids were extracted from the CPB samples by using a pore fluid extractor that is especially engineered for this purpose based on the steel die high pressure technique (Barneyback and Diamond 1981) to investigate the evolution of the ion concentration in the liquid phase within the pores of the CPB. The concentration of various major cations (Mg^{2+}, K^{+}, Al^{3+}, Ca^{2+}, Na^{+}, Fe^{2+}, Si^{4+}) and anions (SO_4^{2-}), and the pH were determined for each sample. The concentrations of the analyzed elements were determined by inductively coupled plasma atomic emission spectroscopy (ICP-AES). Sulphate ion (SO_4^{2-}) concentrations were measured using automated calorimetry.

2.4.5 Microstructural Tests

The microstructure of the studied CPB samples was investigated by MIP and SEM. Although it has some limitations, MIP has been used to evaluate the pore-size distribution (PSD) of cementitious materials for many years (e.g., Cook and Hover 1999; Diamond 2004; Fall and Samb 2008). SEM was carried out with a Hitachi S4800 field emission microscope at different magnifications to study the texture of the CPB and morphology of the cement hydration products. MIP was performed using PMI Mercury/Nonmercury Intrusion Porosimeter instrument to evaluate the pore size distribution and total porosity. Prior to the conducting of MIP and SEM, all of the samples were dried at 50 °C to a constant mass in a vacuum oven to remove the free water. Drying at this temperature did not appear to cause cracking.

3 Results and Discussion

3.1 Evolution of Physical Properties

The evolution of the physical properties including void ratio (e), porosity (n), bulk density (γ) and water content (ω) was measured with time, for the C-ST, CUS-ZnT and CUS-ST samples and the test results are presented in Fig. 5. It can be observed that there is a relationship between the evolution of the bulk properties and curing conditions. From Fig. 5a, it is observed that in all of the samples, the porosity decreases as the curing time increases. This is due to the ongoing cement hydration process and the associated heat generation (Fig. 16) which produce larger amounts of hydration products, which in turn, cause the refinement of the pore structure with time (Fall and Samb 2008). Moreover, the CUS-ST sample shows lower porosity compared to the control sample (C-ST). This is mainly due to the pore refinement as a result of the pressure application. Applied pressure can lead to a more compacted CPB matrix, which in turn, decreases the physical properties, such as porosity. This is experimentally supported by the results of the MIP analyses presented in Sect. 3.6.2 (to be discussed later). Also, the porosity evolution in the CUS-ZnT sample shows the same behavior as that of the CUS-ST. However, the porosity values of the CPB made from Zn-tailings are considerably higher than those of the silica samples, primarily due to the differences in water content, tailings specific gravity and mineralogy (see Tables 1, 2). Figure 5b shows that the gravimetric water content of all the samples decreases with curing time mainly due to the consumption of water as a result of the cement hydration reactions. The water content variation of the CUS-ST and C-ST samples is almost the same. This means that pressure application has no significant effect on water content variation in undrained loading conditions. However, the water content of the CUS-ZnT sample is considerably reduced with curing time. The overall trend in Fig. 5c shows that the dry bulk density (γ_{dry}) increases with curing time. The dry bulk density at 7 days of curing shows a higher value compared with 1 day of curing. This is due to the refinement of the pore structure (Fall et al. 2009) and reduction of the void ratio or porosity (Fig. 5a) as the pore voids are filled with cement hydration products in the cemented matrix, which eventually produce a CPB material with a higher dry density. Moreover, the dry bulk density of CUS-ZnT shows a lower value compared to that of the CUS-ST. This is attributed to the higher void ratio and porosity of the CUS-ZnT (Table 4; Fig. 5a) and therefore, lower dry bulk density. However, curing under stress tests conducted on CPB made of both ST and ZnT followed the same qualitative behavior. It can be observed from Fig. 5d that there is a direct relationship between water content and the void ratio for a degree of saturation above 80 %. The void ratio decreases with water content for all of the test series. In considering that CPB with higher water content will have a greater void volume that is filled with water and therefore higher void ratio (Fall et al. 2008). This behavior was observed for both types of tailings.

3.2 Evolution of the Mechanical Properties

3.2.1 Unconfined Compressive Strength

The UCS test results showed that the UCS values for all of the samples increase with curing time (Fig. 6). The reason for this behavior is an increase in the degree of cement hydration with time and the associated refinement of the pore structure of the CPB (due to the precipitation of a larger amount of hydration products), and self-desiccation induced suction increase within the CPB (Figs. 7, 14). This time-dependent increase in the degree of cement hydration

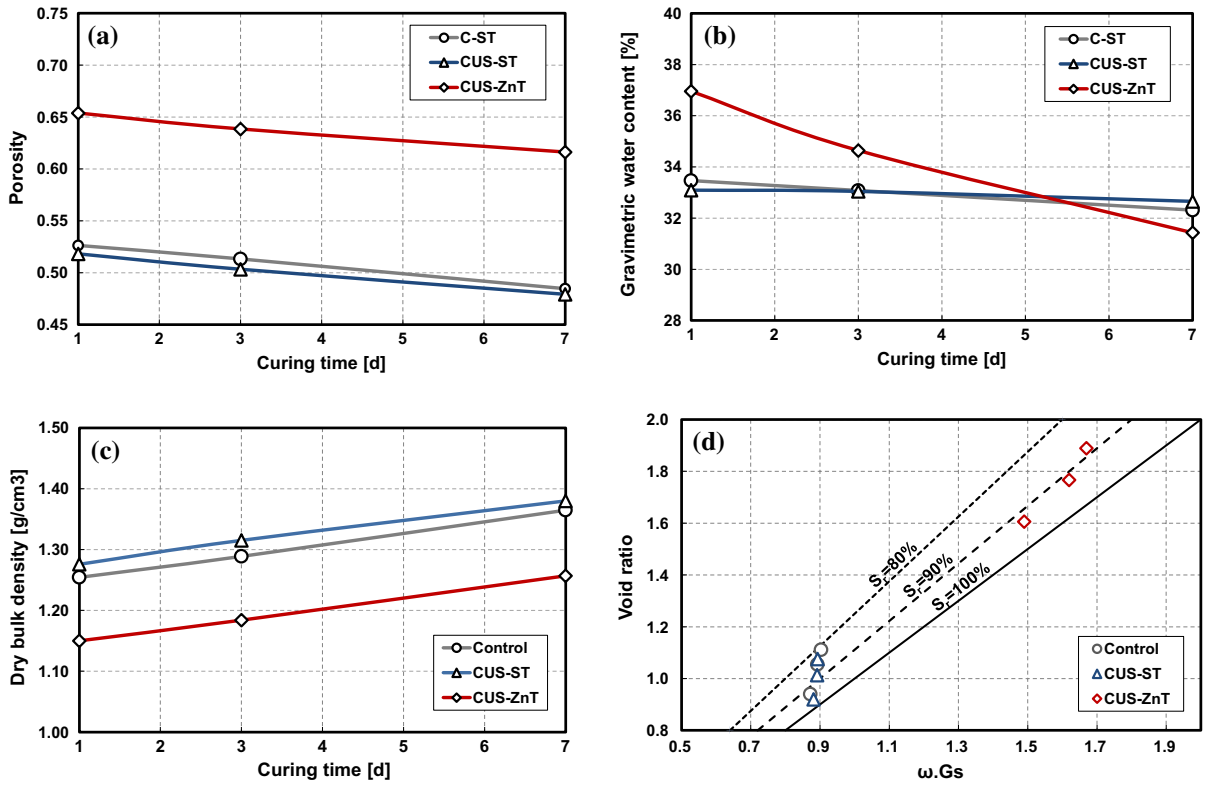

Fig. 5 Evolution of the physical properties: **a** porosity; **b** gravimetric water content; **c** dry bulk density; and **d** void ratio versus water content based on multiple specific gravity

and the associated refinement of the pore structure have already been demonstrated by several previous studies (e.g., Taylor 1997; Espinos and Franke 2006; Fall and Samb 2008). When compared to the C-ST samples (control), the CUS-ST samples exhibited considerably higher compressive strength. This can be explained by the effect of the pressure application on the microstructure or pore structure changes. Curing under stress increases the packing density of the material through decrease in total porosity and void ratio (Fig. 5), which results in denser pore structure (Fig. 20). This decrease in porosity and a denser pore structure leads to compressive strength gain (Fall et al. 2005). An additional factor could be suggested as a contributor to the stress induced strength increase of CPB at early ages. This factor is the curing stress induced increase of cement hydration degree at early ages (Zhou and Beaudoin 2003).

From Fig. 6, it can be also observed that the CUS-ZnT samples exhibited a much lower mechanical strength than that of the CUS-ST samples. This

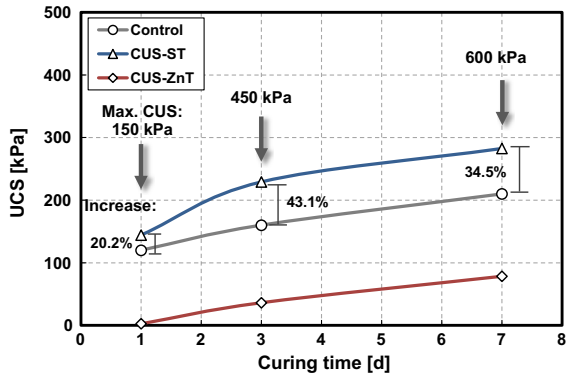

Fig. 6 Effect of curing under stress on UCS development

observation confirms the importance of the physical properties (e.g., specific gravity, strength of the tailings particles) and mineralogical composition/chemistry of the tailings (see comparison in Table 1), and the chemical composition of its pore water (see comparison in Table 6) in the response of the CPB. This strength difference is attributed to the

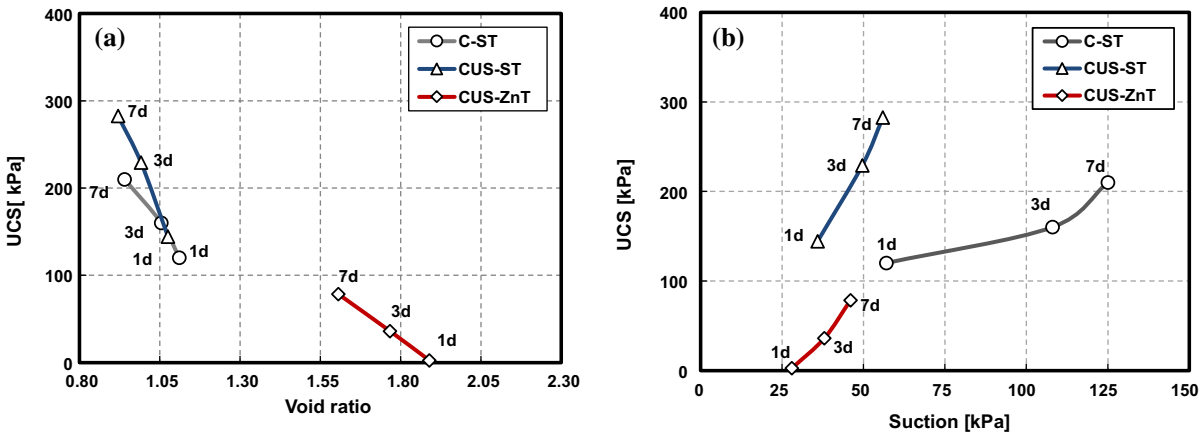

Fig. 7 Evolution of **a** UCS versus void ratio; **b** UCS versus suction

combined effects of the aforementioned factors that are related to the tailings and its pore water chemistry. The specific gravity of ZnT (3.34) is higher than that of ST (2.70) (Table 2). Thus, for a given *w/c* ratio (7.6 in this study), CPB made of ZnT will have a higher initial void ratio (1.92) or porosity than the samples made of ST (1.15; Table 4; Fig. 5a). It is well known that, for a given type of CPB or porous medium, the strength often decreases as the void ratio or porosity increases (e.g., Kesimal et al. 2003; Fall et al. 2010a; Ercikdi et al. 2013) as demonstrated in Fig. 7a (will be discussed later). In fact, there is evidence which confirms that the aggregate mineralogy and chemistry influence Portland cement based materials due to chemical interactions between the aggregates, and the cement pore fluid and cementitious matrix as demonstrated in previous studies (e.g., Pacheco-Torgal et al. 2007). However, it should be emphasized that this subject still requires further extensive studies to provide a complete understanding of the interactions between tailings type and hydration of cement as well as the importance of the mineralogical and chemical properties of tailings on the strength development of CPB. An additional factor that contributes to a lower strength of the CUS-ZnT is attributed to the relatively high concentration of sulphate present in the pore water of the ZnT (Table 6). The presence of chemical elements, especially sulphate, can significantly inhibit binder hydration (e.g., Tzouvalas et al. 2004; Fall and Pokharel 2010) and thereby slow down the strength development inside the backfill (Fall and Benzaazoua 2005). Furthermore, sulphate induced inhibition of cement hydration results in lower generation of heat within the CUS-ZnT samples than within the CUS-ST samples as shown by Fig. 16. It is well established that the curing temperature can significantly increase the rate of early age strength gain and strength of the CPB (Fall et al. 2010a).

From Fig. 7a, it is seen that the UCS value increases while the porosity decreases. A strong correlation between the evolution of the UCS and porosity reduction as the result of the refinement of pores is noticeable. Due to the cement hydration process, capillary pores in the CPB matrix are filled with cement hydration products and hence the porosity decreases with time (Fall et al. 2009). This process leads to a denser matrix and increase in the UCS values. The test results are supported by the SEM images and MIP results which will be discussed later. From Fig. 7b, it can be noticed that an increase in suction leads to an increase in the UCS values in all of the samples, or in other words, there are H–M coupled

Table 6 Chemical composition of pore water of zinc tailings

Elements	pH	Sulphate (mg/l)	Al (mg/l)	Ca (mg/l)	Fe (mg/l)	Mg (mg/l)	K (mg/l)	Si (mg/l)	Na (mg/l)
ZnT	5.3	2600	2.2	60,000	19	2300	200	15	53

processes. Suction development as a result of self-desiccation can lead to an increase in the backfill strength (e.g., Abdul-Hussain and Fall 2011). Suction development can decrease the pore pressure and thus increase the effective stress inside the backfill. It is seen that both effect of applied pressure and suction are noticeable on strength growth. However, the contribution of pressure application is higher than that of suction (Fig. 7b).

3.2.2 Stress–Strain Behavior

The stress–strain properties of the CPB samples were investigated for different curing times. As can be seen from Fig. 8a, the shape of the stress–strain curves is affected by the curing time. For example, the peak stress is achieved for large strain values of the CPB samples at 1 day compared to 7 days for both the C-ST and CUS-ST samples. The slope and shape of the stress–strain curve of both C-ST and CUS-ST samples at 1 day curing change with increases in the UCS values. Also, the CPB samples at a very early age (1 day) for both C-ST and CUS-ST show a plastic behavior, but transitions into less "plastic" deformation at 7 days which corresponds to the higher UCS values. The aforementioned behavior is due to the fact that the CPB sample at 7 days has a higher value in strength and hence can absorb more energy up to the peak stress compared to the 1 day sample. This could result in the propagation of cracks and rapid deformation at the time of failure, and therefore, a sharp reduction in the stress–strain curves (Fall et al. 2007). Furthermore, the curing pressure has no significant impact on the shape of the stress–strain curve of the CPBs studied. For example, the C-ST and CUS-ST samples at 7 days have relatively "brittle" behavior. It is interesting to note that the CUS-ZnT sample at 7 days of curing showed a very plastic behavior compared to the CUS-ST sample at the same age. This underlines again the importance of the physical characteristics and mineralogy/chemistry of the tailings and its pore chemistry, and their consequences on the cement hydration process and the amount of heat generated on the mechanical behavior of CPB as discussed above.

Figure 8b shows the evolution of the modulus of elasticity (E) acquired from the stress–strain curve of the UCS results at different curing times. It can be observed that as the binder hydration progresses or the curing time increases, the E value increases for both the C-ST and CUS-ST samples. Also, it is seen that the effect of the pressure application is noticeable for the CUS-ST sample at 7 days of curing. This is attributed to the fact that backfill with higher cohesion exhibits higher modulus of elasticity (Hassani and Archibald 1998). Since curing stress improves the cohesion (Fig. 9a), a higher modulus of elasticity can be expected. Due to the very low UCS values of the samples prepared with zinc tailings, the modulus of elasticity of the CUS-ZnT samples cannot be reported.

3.2.3 Shear Strength Parameters

The shear strength parameters, including internal friction angle (φ), and cohesion (c), were determined

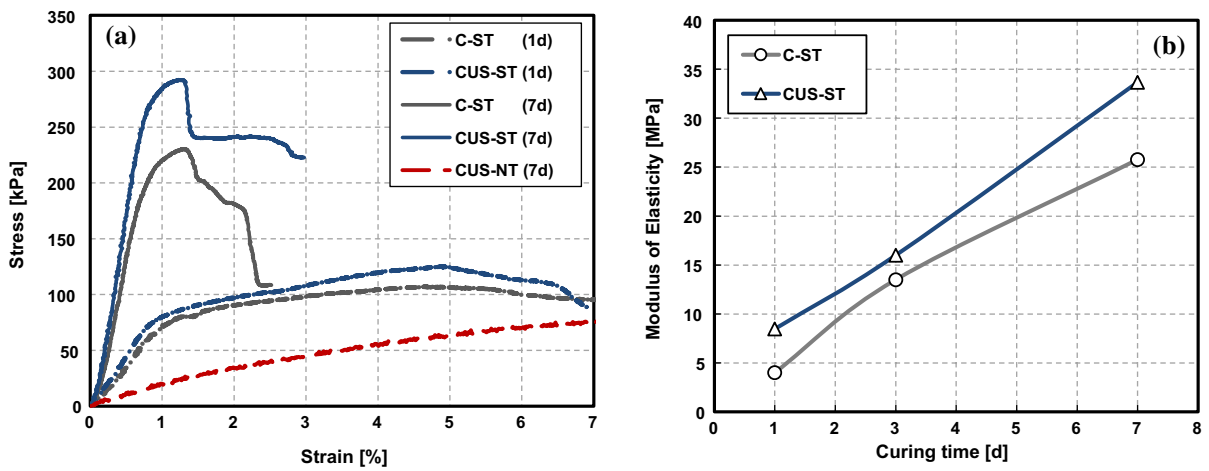

Fig. 8 Effect of curing under stress on: **a** stress–strain behavior; **b** modulus of elasticity

from direct shear tests (Fig. 9). From Fig. 9b, it can be seen that there is no major change in the φ values with time for all of the samples. The average value of φ is 39.6° and 34.7° for the ST (control and CUS) and ZnT samples, respectively. The cohesion (c) of the C-ST and CUS-ST samples ranges from 30 to 70 and 40 to 110 kPa, respectively. This finding shows that both c and φ considerably contribute to the development of the shear strength. However, the time dependent evolution of the shear strength mainly depends upon the development of c rather than φ in the long-term behavior. Similar observations were made by Rankine et al. (2001). This can be explained by the fact that CPB at an early age has weak cementation and instead, internal friction between the tailings particles plays a role in the shear strength development of backfill (le Roux et al. 2005). The lower mean value of friction angle of the ZnT samples compared with the ST samples is related to the differences in tailings type and lower mechanical strength which can result in the reduction of the friction angles.

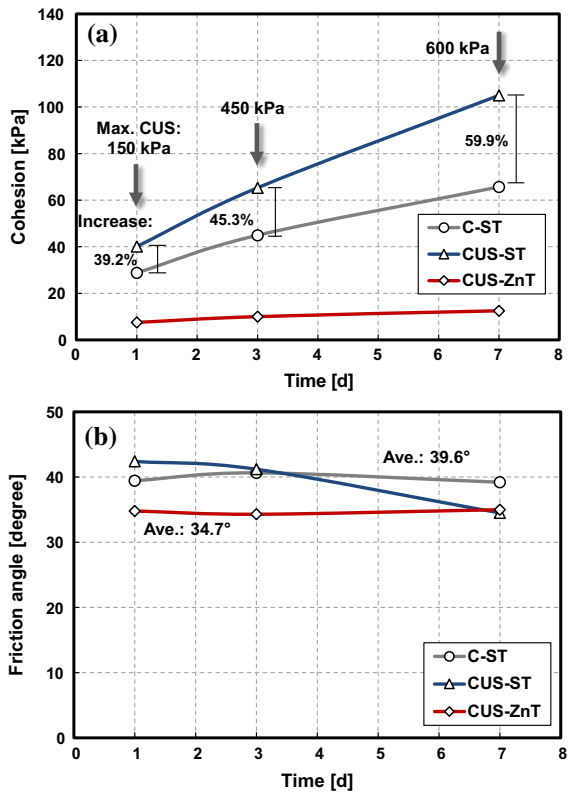

Fig. 9 Effect of curing under stress on shear strength properties: **a** cohesion [C] and **b** friction angle [φ]

Moreover, it should be noted that pressure application has considerable effects on cohesion improvement (Fig. 9a). This behavior is attributed to the curing stress induced refinement of the pore structure or densification of the CPB. The effect of curing stress on the cement hydration could be considered as an additional factor that contributes to this observed behavior (Zhou and Beaudoin 2003). However, it can be observed that pressure application has no major impact on friction angle improvement of the studied CPBs. Similar observations were made by Ahnberg (2007) who conducted triaxial tests on soils stabilized with cement.

3.2.4 *Deformation*

Figure 10 illustrates the results of vertical deformation with time as well as the load-deformation curves. In the case of the CUS-ST test, during the first 12 h, the deformation considerably increases up to 3.2 mm which corresponds to a vertical pressure of 150 kPa. This is followed by lower increments up to 3.63 mm within 24 h and eventually maintains almost a straight line with time. The same qualitative behavior can also be observed in the zinc tailings. However, due to a higher initial void ratio and the chemical and mineralogical characteristics of the tailings and pore water, lower strength and longer setting time (the latter is observed from the electrical conductivity, Fig. 18), and higher deformation was observed when compared with the CUS-ST test.

This measured CPB deformation is mainly due to the combined effects of three factors as follows: (1) the rearrangement of the tailings particles; this rearrangement takes place within a few hours after placement (0–3 h in this study; see Fig. 11). Fresh CPB has relatively high unbound water and high solid density, in which the tailings are suspended in the paste (Landriault 2001). Any pressure application (e.g., self-weight pressure generated in the field backfill) can rearrange the tailing particles, which in turn, can cause large deformations shortly after placement, (2) self-desiccation induced shrinkage (chemical shrinkage); this is linked to the cement hydration process and the consequence of the lowering of the internal relative humidity (RH) in the CPB as capillary or loosely bound water is consumed by the cement reaction. It is well established that the progress of the cement hydration reaction induces decreases in the internal

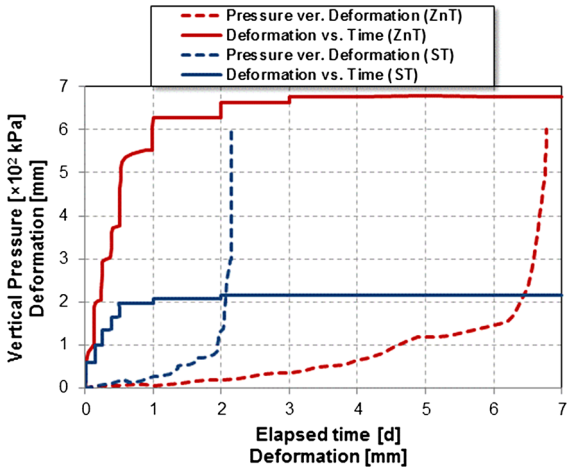

Fig. 10 Vertical pressure versus deformation; and deformation versus curing time

RH within the hydrating cementitious system (this is evidenced by the evolution of the pore water pressure or suction shown in Fig. 14), thus resulting not only in the formation of a solid skeleton of the CPB (hereafter simply referred to as solid skeleton) with filled and refined coarse capillary spaces, but also air-filled spaces (Meddah and Tagnit-Hamou 2011) (Fig. 11). Hence, a decrease in the RH results in an increase in the capillary pressure. A consequence of increasing capillary pressure is the growing compressive pressure exerted by the pore fluids onto the solid skeleton. This pressure results in negative strains of the solid skeleton, i.e., shrinkage strains (Gawin et al. 2007), (3) thermal shrinkage, which is the volume reduction of the CPB due a decrease in the binder hydration induced temperature after the CPB reaches its peak temperature. This decrease in temperature after the peak is illustrated in Fig. 16. Similar observations have been made in concrete materials (e.g., Meddah and Tagnit-Hamou 2011).

These findings with regards to self-desiccation induced volume change suggest that, even in undrained conditions (i.e., no dissipation of excess of pore water pressure by drainage), the CPB structure can be subjected to consolidation at early ages. However, it should be emphasized that due to the undrained conditions that govern the whole system, this consolidation mechanism (self-desiccation induced consolidation) is not similar to the conventional consolidation mechanism known in soil mechanics where excess pore water can be drained out by applied pressure. In fact, water is drained by the self-desiccation process from the micro-pores due to cement hydration reactions. This is the period (3–48 h in this study) in which the backfill setting takes place (transformation from paste to formation of solid skeleton; Fig. 11). In this period of time, reduction in pore pressure (development of suction) due to self-desiccation and development of effective stress occur in the backfill. Mechanical properties (e.g., strength, stiffness) can be built up and hence the voids can no longer be significantly affected by the applied pressure in this study. Therefore, vertical deformation reaches an almost constant value after the setting time. The

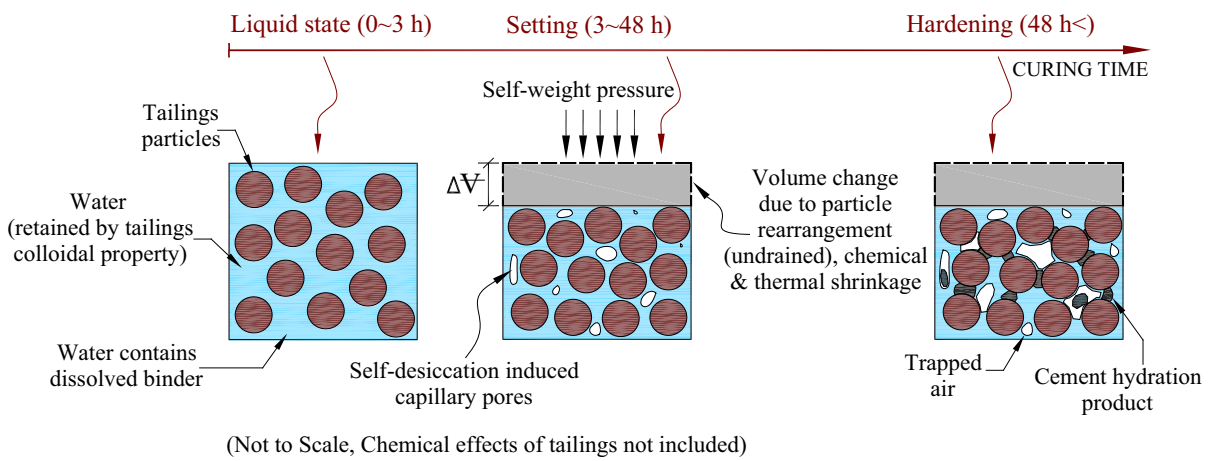

Fig. 11 Schematic presentation of the coupled effect of cement hydration, self-desiccation and pressure application in the studied CPB at early ages and in undrained conditions

period after 48 h can be considered as the hardening process. Continual growth of cement hydration products, strength development and no further significant volume changes are the key properties of the backfill during this period of time.

3.3 Evolution of Hydraulic Properties

3.3.1 Hydraulic Conductivity

The evolution of the saturated hydraulic conductivity (k_{sat}) with curing time is shown in Fig. 12. It is seen that the values of k_{sat} decrease with time for all of the samples. This decrease in the k_{sat} is due to the refinement of the pores as a result of the cement hydration process. This is evidenced by Figs. 5a and 13a, which confirm that, as the curing time advances, the void ratio decreases (Fig. 5a), which results in lower k_{sat} values (Fig. 13a), regardless of the curing conditions (stress-free or under stress). Reduction in capillary porosity during hydration and a denser cemented matrix eventually reduce the fluid transportability of the CPB. Similar observations and conclusions have been made in several previous studies (e.g., Godbout 2005; Fall et al. 2009). However, from Fig. 12, it can be noticed that the k_{sat} is not only controlled by the evolution of the void ratio due to the progress of binder hydration, but other factors, such as applied pressure, can significantly decrease the hydraulic conductivity. A comparison of the k_{sat} values in the C-ST and CUS-ST samples showed that pressure application has a significant effect on hydraulic conductivity values. When compared to the control test, the CUS-ST samples show a decrease in hydraulic conductivity of 65, 77 and 78 % for curing times of 1, 3 and 7 days, respectively. Also, the CUS-ZnT sample shows similar behavior as the CUS-ST sample in terms of the effect of pressure application which results in decreased saturated hydraulic conductivity. This pressure induced decrease in hydraulic conductivity is explained by the fact that the curing pressure contributes to reducing the void ratio or porosity of the CPB, and thus the hydraulic conductivity. A lower void ratio of the CUS-ST sample compared with the C-ST sample at the same curing time supports this statement (Fig. 5a). The reason for the decrease of the CPB void ratio is because of the curing stress, which has already been explained in the previous section. This observation is confirmed by the MIP tests conducted on the C-ST and CUS-ST samples at 7 days of curing which will be discussed later. Based on the MIP results, lower hydraulic conductivity was observed on samples with lower porosity, lower threshold diameter and finer PSD (Fig. 20). As evident in Fig. 13b, there is a strong relationship between the UCS and the hydraulic conductivity of the backfill at any curing time.

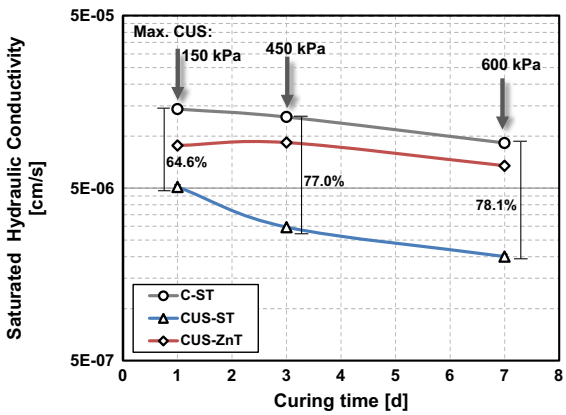

Fig. 12 Effect of curing stress on saturated hydraulic conductivity evolution

3.3.2 Pore Pressure and Suction Response

The designing of a safe and stable barricade erected on the draw-point of a mine stope is one of the most important design aspects of the CPB. For this purpose, an understanding of backfill behavior in terms of pore pressure (u), suction and evolution of effective stress (σ') is of foremost importance for designers. This is especially true in the early hours of backfilling, when the pore pressure development at the draw-point is important and its theoretical evaluation is highly dependent on variable factors, such as backfill hydraulic conductivity, rate of self-desiccation, drainage, consolidation, arching effects and cement hydration (Fall et al. 2009; Li and Aubertin 2009).

The total pressure, cumulative pore pressure reduction and suction data obtained from installed sensors for a period of 7 days are shown in Fig. 14 for the CUS-ST and CUS-ZnT samples. The minimum detectable reading of the suction meter is −12 kPa. Therefore, the suction reading obtained for the C-ST sample started from this value at about 13 h of curing. However, it should be noted that the onset of suction

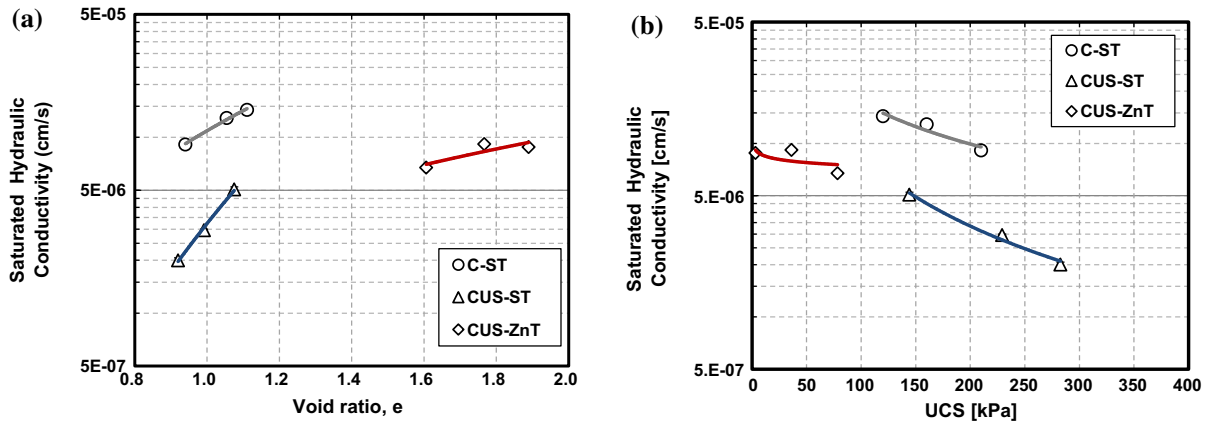

Fig. 13 **a** Saturated hydraulic conductivity versus void ratio, **b** relationship between UCS and saturated hydraulic conductivity

(PWP = 0 kPa) started at an earlier time, about 3–4 h after loading. For the C-ST sample, rapid evolution of suction could be observed during the first 24 h of curing, followed with a lower rate of suction development from 24 to 72 h. After 3 days and up to 7 days, very low evolution of suction can be noticed. This is attributed to the lower rate of cement hydration reaction (lower rate of self-desiccation) associated with lower rate of pore refinement within this period of time. The maximum value of the suction at 7 days of curing is about 110 kPa for the C-ST sample.

In terms of samples cured under stress (UCS-ST and UCS-ZnT samples), the pressure was gradually increased every 3 h up to 150 kPa for the first 12 h after the CPB placement. Then, the pressure increment was 150 kPa for the next 12 h and then 150 kPa per day up to 600 kPa (Fig. 3). The increments of the curing pressure can be observed in the total pressure (TP) curve. The obtained results have shown that the

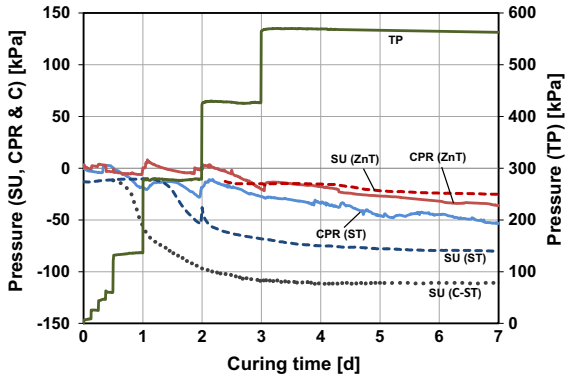

Fig. 14 Sensor readings, *TP* total pressure, *CPR* cumulative pore pressure reduction, *SU* suction

pore pressure gradually increased according to the applied pressure up to 65 kPa during the first 9 h of curing. This pressure increment corresponds to a pressure application of 75 kPa during this period of time. The pore pressure was considerably high in the early hours of curing. This is an indication of low effective stress at very early ages and the existing high pore pressure since the backfill behaves almost like a fluid. However, due to self-desiccation as a result of cement hydration, the pore pressure declined after about 6 h and 2 days for CUS-ST and CUS-ZnT, respectively. Moreover, the results of the cumulative pore pressure reduction (CPR) are presented in Fig. 14. Rapid development of negative pore pressure (suction) started after 6 h and 2 days for CUS-ST and CUS-ZnT, respectively. It is noticed that the development of suction is affected by the sequence of pressure application. For example, in the CPR curve for the ST sample, the pressure increments at first and second days caused a significant rise in the pore pressure and then gradually started to decrease. The pressure increment at third day and after had not an important influence on CPR curve (Fig. 14). It is attributed to the fact that backfill pore structure reached to a hard matrix and cannot be consolidated by the pressure application. Pressure increase excited the CPR (ZnT) curve to a positive value at both first and second days of curing. This means that effective stress and associated strength gain could not strongly develop in the ZnT samples up to about 2 days of curing. This can be observed from the UCS results of the CUS-ZnT samples at 1 and 3 days which exhibited very low strength in the early days of curing. These observations suggest that differences in tailings

mineralogy and chemistry (CUS-ST, CUS-ZnT) can significantly affect the hydration behavior, and hence the PWP evolution within a CPB.

The obtained results also shown that after each pressure increment at 2 and 3 days of curing, the pore pressure curves for CUS-ST and CUS-ZnT samples were considerably lower than the total pressure curve. This is due to the fact that CPB transforms from a liquid stage (paste) to the formation of a solid skeleton after 6 and 48 h with respect to the CUS-ST and CUS-ZnT samples (Fig. 11), respectively. Therefore, much of the applied vertical pressure is carried by the tailings particles. So, due to the formation of strong bonding between the tailings particles, pressure application will not be able to considerably interrupt the evolution of the pore pressure after this point.

Suction readings obtained from a suction meter for both the UCS-ST and CUS-ZnT samples are also presented in the graph and labeled as SU (ST) and SU (ZnT), respectively. Theoretically, the SU curve should be matched with the CPR curve. Although the suction curves for both the ST and ZnT samples show the same qualitative behavior as the piezometer readings, there are some differences in the actual values. For example, the negative pore pressure obtained from the suction meter shows higher values compared to the corresponding reading obtained from the piezometer which is plotted in a CPR curve. This could be due to the different sensing mechanisms of the sensors. VW piezometer directly measures the water pressure and then converts the water pressure into a frequency signal via a diaphragm; it can be later translated into a numeric value. However, the suction meter has an indirect mechanism; it measures the water content of a porous ceramic disk mounted on top of the sensor and then converts the volume to a suction value by using the water characteristic curve (WCC) of the ceramic disk (MPS-2 manual 2014). The suction reading for the ZnT sample is −25 kPa at 7 days of curing which is considerably lower than that of ST sample which is −80.1 kPa. Further studies should address this issue.

3.4 Evolution of Thermal Properties and Heat Development

3.4.1 Thermal Conductivity Properties

The evolution of thermal conductivity with time was investigated for all of the samples and the results are shown in Fig. 15. It is seen that for samples prepared with silica tailings, the thermal conductivity (k) values slightly decrease as the curing time is increased from 1 to 7 days. This behavior is mainly attributed to the strong coupling between k and the degree of saturation. Indeed, as the curing time increases, the suction of the CPB increases or the degree of saturation decreases because of self-desiccation. This increase in suction is supported by the experimental evidence shown in Fig. 14. The variation in the degree of saturation with time is a main factor that can change the k values (Kim et al. 2003; Celestin and Fall 2009). Since air has lower k than water, desaturation as a result of self-desiccation followed by an increase in air voids can reduce the k of the CPB materials. So, similar to the concrete material reported by Khan (2002), the k of CPB decreases with a decrease in the degree of saturation (Celestin and Fall 2009).

The thermal conductivity of the CUS-ZnT samples shows lower values compared with the ST samples regardless of the curing stress. This is due to the effect of the porosity or void ratio and the mineralogical composition of the tailings on the thermal conductivity. Lower porosity or void ratio leads to denser cemented materials, thereby to higher thermal conductivity (Khan 2002; Celestin and Fall 2009). The void ratio (and porosity) of the CUS-ZnT samples is considerably higher than that of the C-ST and CUS-ST samples, which in turn, present lower k values (Fig. 5a). The experimental tests performed by Celestin and Fall (2009) have revealed that the mineralogical composition of tailings or the proportion of quartz present in the tailings materials has a significant

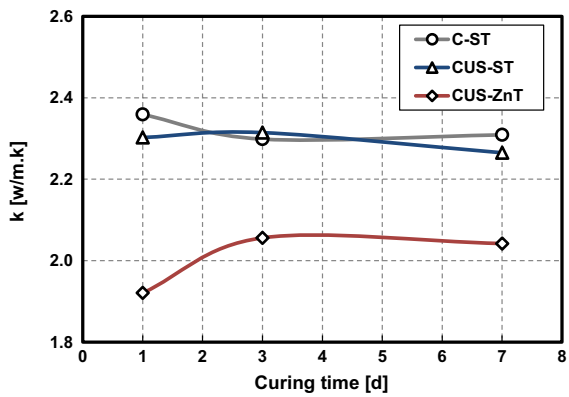

Fig. 15 Effect of curing under stress on the evolution of thermal conductivity

impact on the thermal properties of the CPB. The thermal conductivity of the CPB increases with an increase in the quartz content. This is because the thermal conductivity of quartz is much higher than that of other minerals (e.g., K = 7.7 W/m °C for quartz, 2.25 W/m °C for feldspar, 2.03 W/m °C for mica, and 3.46 W/m °C for amphibole according to Horai 1971) and also other components of CPB (water and cement paste). It is shown in Table 1 that the ZnT tailings contain only 11.9 % quartz whereas the silica tailings (ST) comprise 99.8 % quartz.

Moreover, for the CUS-ZnT samples, the *k* values from time of preparation increased up to 3 days and remained constant. For zinc tailings used in this study, the curing time of 48–60 h can be considered as the time of solid skeleton formation. The electrical conductivity monitoring of the CUS-ZnT samples compared with that of the CUS-ST support this argument (see Fig. 18). During the setting period, the cement hydration products slightly filled the large pores, while unbound water was consumed by cement hydration, which in turn, increased the contribution of the tailings volume fraction on the thermal conductivity (Khan 2002). Between 3 and 7 days of curing, the moisture content (and degree of saturation) in the backfill started to decrease as a result of the associated cement hydration, which in turn, decreased the *k* values up to 7 days.

3.4.2 *Heat of Cement Hydration*

From the temperature evolution curves in Fig. 16, it is seen that all the samples showed qualitatively the same behavior. The temperature increments vary between 2.6 and 3.5 °C. The heat of hydration quickly reaches the upmost value after about 11 and 16 h in the ST (CUS and control) and ZnT samples, respectively. The most important part of the generated heat of hydration can be related to the exothermic reactions of aluminate (C_3A) with gypsum to form ettringite as well as the hydration of tricalcium silicate (C_3S) to form calcium silicate hydrate (C–S–H) (Taylor 1997; Swaddiwudhipong et al. 2002). From the CUS-ST curve, it is seen that there is a significant amount of heat up to 2 days of curing which can contribute to the acceleration of the cement hydration reactions and associated self-desiccation. Between about 2 and 7 days of curing, the CPB sample started to gradually cool down and reached a temperature close to ambient.

The development of suction in the cells had a strong coupled relationship with heat of hydration. As presented earlier in Fig. 14, the evolution of suction for both the CUS-CT and C-ST samples has the highest rate of increase during the first 2 days after placement. The maximum rate of suction development was achieved at the time of utmost temperature, thus supporting that there was strongly coupled T–H behavior in the studied material. This process is stronger when large amounts of CPB are backfilled into a mine stope. In a typical backfill structure, the temperature as a result of hydration can reach 50 °C depending on the binder type and content as well as the size of the filled stope (e.g., Nasir and Fall 2010; Fall et al. 2010a).

By comparing the CUS-ST and C-ST tests, it can be seen that the pressure application has no significant impacts on the temperature evolution of the studied CPBs. The CUS-ZnT sample had less heat of hydration compared to the CUS-ST sample. This lower heat of hydration is attributed to the chemical interactions between the tailings and its initial pore water chemistry, and the cement hydration process. The presence of a relatively high amount of chemical impurities (e.g., sulphate ions; see Table 6) decreased the rate of hydration, which in turn, resulted in lower heat generation. The presence of high quantities of sulphate in the cement matrix significantly retards the hydration reaction of the cement (Pokharel and Fall 2011). It is well known that sulphate strongly inhibits the hydration of C_3A. The hydration of C_3A is one of the major contributors to heat generation during the hydration of a cement system (e.g., Taylor 1997). The retardation

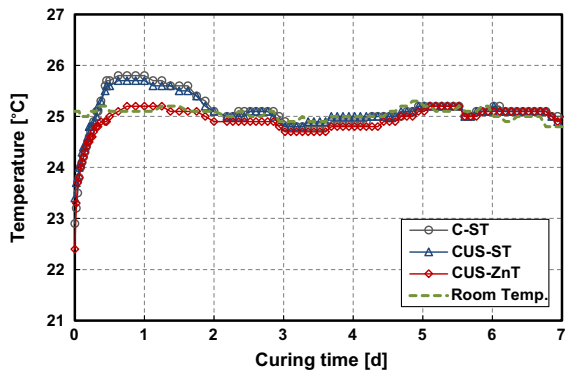

Fig. 16 Evolution of heat of hydration with curing time for different samples

phenomenon can be adequately explained on the basis of the reduced solubility of the C_3A in solutions that are saturated with sulphate (Mehta and Monteiro 2013).

3.5 Evolution of Chemical Properties

3.5.1 Pore Fluid Chemistry

To understand the chemical evolution of CPB and its relationship to the THM factors, the concentration of some important cations, such as potassium (K), sodium (Na), calcium (Ca), magnesium (Mg), aluminum (Al), iron (Fe) and silicon (Si), as well as anion concentration, including SO_4, are investigated in this study. CPB as a cement-based material gains strength with the formation of various specific cement hydration products (e.g., C–S–H, CH) (Fall et al. 2010a). When water is added to CPB, the cement clinker that contains four primary types of minerals (i.e., C_3S, dicalcium silicate (C_2S), C_3A and ferrite (C_4AF)) releases some ions into the pore solution (Double 1983). This process will change the anhydrous compositions to hydrated products, which is mainly called a cement hydration reaction. The process ultimately ends up with the precipitation of three important cement hydration products, including C–S–H, calcium hydroxide (CH) and ettringite (Hansen et al. 1973). The results of the obtained chemical analysis of the pore solution are shown in Fig. 17. The analysis was conducted on two samples of CUS-ST and CUS-ZnT at 1, 3 and 7 days of curing. The cement hydration reactions commenced with the hydration of the cement clinkers (Double 1983). These processes changed the anhydrous compositions to hydrated products and as a result, the concentration of some ions, such as Ca, Na, K and SO_4, increased in the pore solution. This is the reason that a high concentration of these ions can be noticed in the first 24 h of hydration, see Fig. 17.

The concentrations of Ca and SO_4 are close to 1000 g/l on the first day of curing both the CUS-ST and CUS-ZnT samples. The initial concentrations of these cations depend on the cement composition and *w/c* ratio (Lothenbach and Wieland 2006). The quick dissolution of C_3S, which is the primary anhydrous phase of cement, releases these cations into the pore solution (Taylor 1997). The concentrations of the other cations (Al, Mg, Si and Fe) are considerably lower, between about 1 and 10 g/l.

The pore solution composition considerably changes from day 1 to day 3 of the hydration. The concentrations of SO_4 and Ca are limited by the presence of CH and gypsum (Lothenbach and Wieland 2006). The SO_4 and Ca concentrations decrease during this period of time. The Ca concentrations decrease from 680 to 380 and 1520 to 1120 g/l for CUS-ST and CUS-ZnT, respectively. Also, the SO_4 concentration is reduced from 2400 to 1700 g/l for the CUS-ZnT sample between 1 and 3 days of curing.

The Ca was reduced from the solution to form C–S–H and CH (Benzaazoua et al. 2004). Other cations, such as Al, Fe and Mg, were reacted with SO_4 and OH to produce a greater volume of ettringite and more stable monosulfate (AFm; Lothenbach et al. 2007). These reactions were reflected in the depletion of Fe and Mg from the pore solution up to 7 days of hydration. The same dissolution reaction by C_3S could still take place, although other cement constituents had increased involvement, such as C_3A, and at later stages, by the hydration of C_2S. This results in rapid growth in ettringite and the formation of C–S–H and CH (Taylor 1997; Lothenbach et al. 2007). The rapid reduction in the Ca and SO_4 concentration is considerable due to these reactions.

The concentration of alkalis, such as Na and K, shows slight increases for both the CUS-ST and CUS-ZnT samples between 1 and 7 days of curing. The average concentration of K is about 957 and 1052 g/l for the CUS-ST and CUS-ZnT samples, respectively. Also, for the same period of time, the concentration of Na is 207 and 161 g/l for CUS-ST and CUS-ZnT, respectively. This is attributed to the decrease in the volume of the pore solution as the result of cement hydration and slow release of alkalis from the cement clinker, even when a small portion of these ions was consumed to form C–S–H (Lothenbach and Wieland 2006). The evolution of the CPB strength can be observed from increases in the UCS values at about 53 % from 3 to 7 days for the CUS-ZnT samples. Also, the hydraulic conductivity evolves about 35 % between 3 and 7 days for the CUS-ZnT samples. This indicates the precipitation of C–S–H and CH products with time and shows that a strong coupled relationship exists between the chemical and hydro-mechanical properties of CPB.

The results showed that the pH values did not change considerably during the studied period. The average pH value for the CUS-ST and CUS-ZnT

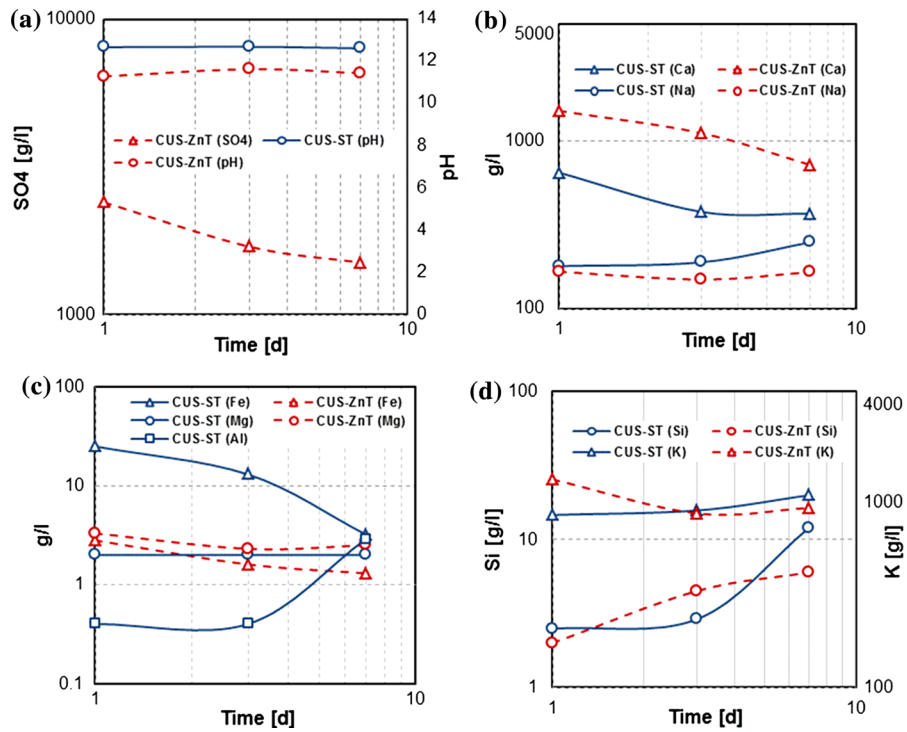

Fig. 17 Evolution of pore fluid chemical concentration with curing time

samples were measured to be about 12.7 and 11.5, respectively. In addition, the pH value of the sample prepared with zinc tailing was lower than that of the ST. This can be attributed to the different tailings mineralogy and chemistry which affect the pH and also initial concentration of ions in the pore solution. However, it should be noted that the same trend for pore solution evolution was observed for both studied tailings which means that similar chemical reactions could have taken place in both pore solutions.

3.5.2 Electrical Conductivity

The electrical conductivity was determined from the dielectric properties of the studied material. The change in ionic concentrations in the pore fluid as a result of cement hydration can be detected by the electrical conductivity of the backfill (Thottarath 2010). From Fig. 18, it is seen that all of the studied samples show the same qualitative behavior. Soon after mixing, the electrical conductivity (EC) started to gradually increase to reach the peak value. This increase in the EC can be explained by an increase of the ion concentration in the pore fluid as well as temperature increase (Fig. 16) as a result of the exothermic cement reaction (Levita et al. 2000). The peak value in the EC curve can be corresponded to the initial setting (transforming from the paste phase to solid skeleton formation) of the backfill. Afterward, the electrical conductivity started to decrease with time which is due to the reduction in unbound water as a result of self-desiccation and less connected capillary pores, which in turn, increase the ion path flow (Levita et al. 2000).

In Fig. 18, the setting time in the sample cured under pressure (CUS-ST) shifts to a longer hydration time compared to the C-ST sample. This means that the setting of the former took place at about 12 h of curing which is longer than that of the latter (6 h). This results from the effect of the applied pressure on the excess pore pressure in the CUS-ST sample. Samples cured under stress experience relatively high pore pressures in the early hours of curing (compared to the C-ST sample), which in turn, need more time for setting to occur. Therefore, the setting of CPB which is related to the onset of effective stress requires a longer time. Moreover, the CUS-ST sample exhibits a considerably lower conductivity value after about 4 days of curing compared with the C-ST sample. This is due to the fact that the applying of curing pressure

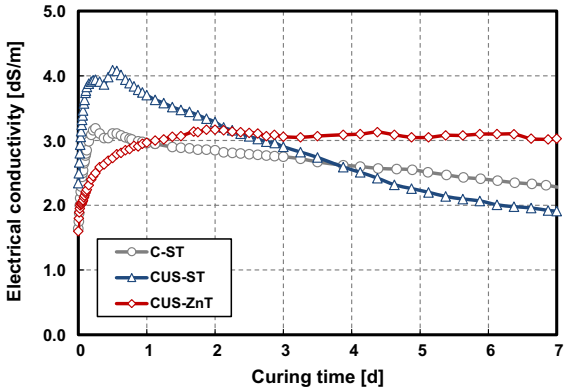

Fig. 18 Evolution of electrical conductivity with curing time

leads to tailings rearrangement and hence, higher packing density of the tailings particles. This causes reduction in the total porosity (Fig. 5a) and void ratio of the CPB (Fall et al. 2005). Therefore, less connected capillary pores as explained above can result in the increase of tortuosity and longer flow path for ions and therefore reduction in the electrical conductivity.

The CUS-ZnT sample shows a very prolonged EC peak value at about 2 days of curing. After the peak value, the EC remains almost constant at around 3 ds/m, which means that cement hydration reactions took place at much slower rates compared to the CUS-ST sample. This behavior can also be supported by the UCS test results. The UCS values for 1 (and also 3 day) cured samples indicate a very low strength and after 7 days of curing, the UCS values of the CUS-ZnT sample are considerably lower than those of the CUS-ST sample. This slower cement hydration rate could be explained by the chemical interactions between the: (1) cemented matrix of the CPB with the tailings; and (2) the cemented matrix of the CPB and its pore solutions as explained earlier. This underlines again the importance of the tailings type in the THMC response of CPB. This subject requires further investigation.

3.6 Pore Structure

3.6.1 SEM Images

The pore size distribution, pore shape and porosity are important microstructural characteristics that can affect the thermo-hydro-mechanical performance of CPB. To understand the effect of curing under stress on the pore structure, samples cured with and without pressure application at 7 days of curing time were used to conduct the SEM. Typical results are presented in Fig. 19. It is seen that two types of pore spaces can be distinguished. The interconnected pores within the CPB structure which can transport fluid across a medium (Dullien 1992) versus the isolated pores that are dispersed over the CPB structure. It is seen that in the C-ST sample, most of the large pores are connected by interconnected micro paths and relatively large connected capillary pores are observed from the SEM images. Capillary spaces between the solid particles are de-saturated as the result of self-desiccation and therefore cause suction development inside the CPB matrix. This mechanism leads to the removal of some of the water out of the saturated voids during the cement hydration reactions and hence interconnected capillary pores can be observed in these images (Fig. 11). These capillary pores will be filled with hydration products (e.g., C–S–H and CH) at advanced ages of curing. The high connectivity of the pores creates capillary networks that act as internal water paths which cause higher tortuosity, thus reducing the hydraulic conductivity (Dullien 1992).

The SEM image of the CUS-ST sample shows that the curing pressure considerably refines the pore structures, see Fig. 19. The tailings particles are more bonded and cement hydration products surround the tailings particles. The pores between the tailings are filled with cemented products, which create a dense matrix with filled intergranular spaces. A few isolated connected pores as well as a much denser and compacted structure can be seen in the CUS-ST sample. This can be explained by the fact that the development of self-desiccation as well as pressure application disconnects the capillary pore networks. Therefore, higher shear strength parameters and lower hydraulic conductivity as reported in the H–M results presented before can be expected. Moreover, the most prevalent cement hydration products formed at early ages are ettringite, with less CH and C–S–H growth as observed by Ghirian and Fall (2013).

3.6.2 MIP Results

The MIP tests were carried out on samples made of silica tailings and cured for periods of 7 days with and without pressure application. This allows us to understand the effect of cement hydration and curing under

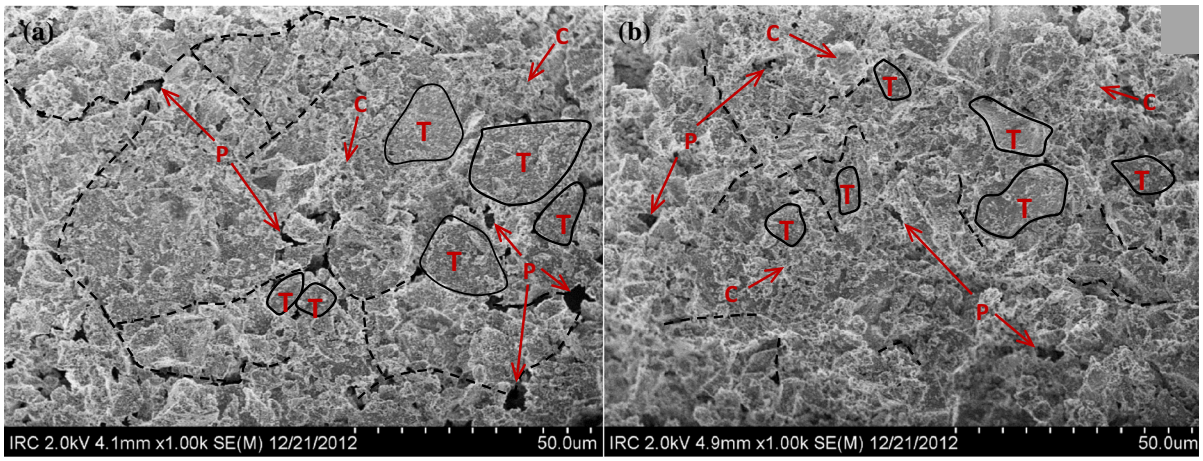

Fig. 19 SEM images show effect of curing under pressure on CPB microstructure at 7 days of curing time **a** without pressure (C-ST); **b** with pressure (CUS-ST). *P* capillary pores, *T* tailings particle, *C* cement products; *dashed line* interconnected pores

stress on the CPB pore structure. Also, the result can be used to investigate the effect of curing stress on the H–M evolution of CPB. Typical MIP results are shown in Fig. 20 and presented in increments for the mercury intrusion porosity and total pore volume.

Figure 20a shows the changes in critical diameter (d_{cr}) and threshold diameter (d_{th}) as a result of pressure application for both the CUS-ST and C-ST samples. The critical diameter (the pore size that corresponds to the maximum mercury intrusion) for both samples is presented. The critical diameter is reduced from 2.29 μm for the C-ST sample to 1.33 μm for the CUS-ST sample. This is attributed to the coupled effect of filling of very fine pores with cement hydration products and pressure application which reaches the dense and finer pore structure. The threshold diameter (d_{th}) is the largest pore diameter at which mercury starts to continuously intrude into the pores (Manmohan and Mehta 1981). It is seen that, based on the MIP results, the threshold diameter is reduced when curing pressure is applied. For the CUS-ST sample, the threshold diameter is 7.42 μm and after pressure application, this value is reduced to 4.61 μm. This means that CPB cured under pressure has lower fluid transportability as demonstrated in Fig. 12. For example, a 37.9 % reduction in the threshold diameter results in a 78.1 % reduction in the saturated hydraulic conductivity (Fig. 12) for a 7 day cured sample. This is caused by the refinement of the pores and a denser CPB matrix (Fig. 5) as well as smaller capillary networks which can result in the H–M improvement of CPB material.

Figure 20b shows that the pore size distribution of the CPB cured under pressure (CUS-ST) is finer than that of the specimen cured without pressure (C-ST). The incremental pore size distribution curve shifts toward a finer pore diameter as a result of curing pressure application. This can result in lower porosity and higher density as observed in the examination of the physical properties. Also, it is observed that the CPB cured under pressure has a finer pore structure. The volume of the macro-pores that are less than 1 μm in size for the CUS-ST sample is 57 % compared with the C-ST sample which is 15 %. This clearly shows the effect of curing under stress on pore refinement. The SEM images of the 7 day sample also demonstrate that after pressure application, the CPB matrix becomes very dense and less permeable.

3.7 Discussion on Coupled THMC Processes at Early Ages

THMC coupled processes in backfill materials are governed by the evolution of different important factors, including the heat of cement hydration (T), pore pressure (H), mechanical strength (M) (e.g., settlement) and chemical reactions (C). Figure 21 shows a schematic diagram of the THMC coupled processes (without the effect of the chemical alteration of tailings) at early ages (curing time $\leq$7 days), which were obtained from the monitoring of the CUS-ST samples. Each curve in this graph represents one process in the system, and is developed based on the

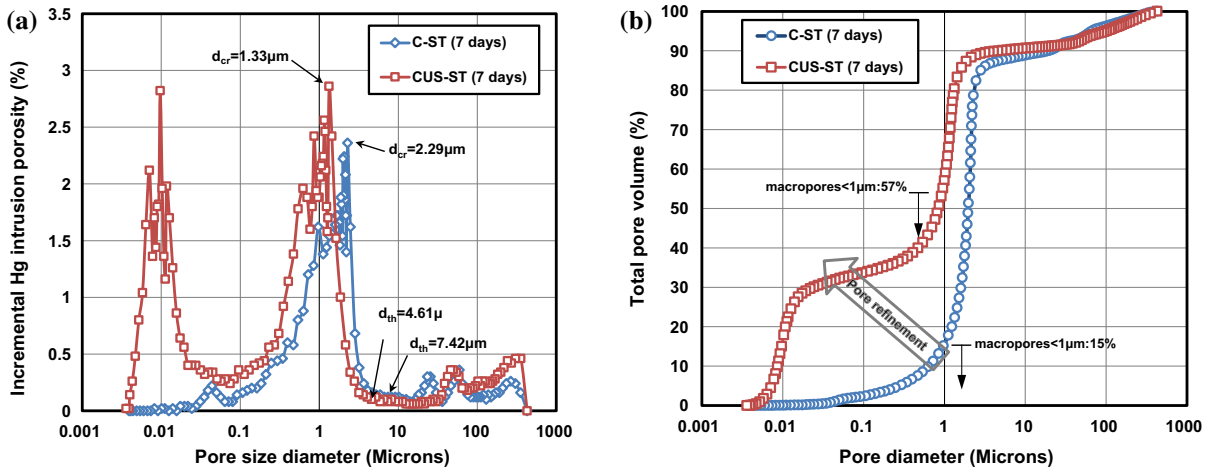

Fig. 20 MIP test results for CUS-ST and C-ST samples: **a** incremental mercury intrusion porosity; and **b** total pore volume

experimental data gained from the CPB monitoring. Different stages in the evolution of the THMC processes can be observed from the graph. Right after the placement of backfill in the cell apparatus, the temperature started to increase due to the exothermic nature of the cement reaction. The peak value of the temperature was obtained at about 12 h of curing. The hydration of C_3A and C_2S in addition to the ongoing hydration of C_3S was primarily the responsible mechanism for increasing the temperature to the peak value (Swaddiwudhipong et al. 2002). Simultaneously, different factors, such as electrical conductivity, as an indication of chemical reactions, started to increase and reached a peak value after about 12 h. In addition, the deformation rapidly increased while the applied pressure was increased during the first early hours of curing. The large deformation in this period is due to the rearrangement of tailings particles under pressure application which causes large volume changes in the backfill as explained earlier. The addition of a large amount of water during the backfill preparation causes very plastic behavior in the CPB materials at early ages. It is interesting to mention that the electric conductivity (EC) peak value took place almost at the same time of the temperature peak, which means that the generated heat of cement hydration can considerably accelerate the cement reactions. This can be observed by an increase in the EC value as a result of the increase in ion concentration in the pore solution. Also, after about 12 h of curing, the negative pore pressure started to concurrently develop with the

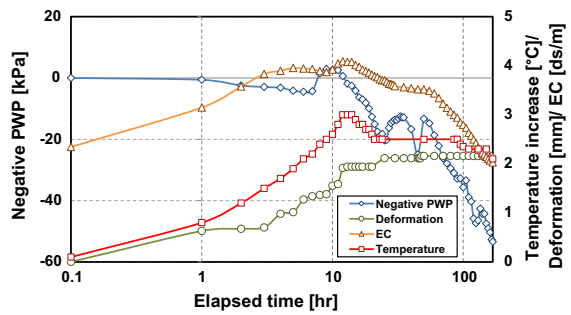

Fig. 21 Schematic diagram of THMC coupled processes in pressure cell experiments at early age (CPB prepared with silica tailings)

temperature peak. This shows coupled T–H behavior. Such coupled interactions can lead to the transition of backfill from the liquid stage to solid skeleton formation; mainly due to the bonding of the tailing particles by the precipitation of the hydration products as well as the development of capillary pressure due to self-desiccation (see Fig. 11). In this study, the age of 12 h of the backfill (CUS-ST sample) can be considered as the maximum contribution of THMC processes in solid skeleton formation. A curing time of 48 h can be considered as the period of solid skeleton formation, since the response to pressure increments from 300 to 450 kPa at 48 h of curing is only a negligible deformation in backfill materials, which means that by the onset of solid skeleton formation, any further pressure can be truly supported by the backfill formation (i.e., matrix of tailings and cement

products). After 48 h, a rapid development in suction was noticeable. The effective stress started to significantly develop as a result of the reduction in pore pressure. Cement reactions consumed the large water filled capillary voids and at the same time, the cement hydration products gradually filled the voids (Abdul-Hussain and Fall 2012). This process caused rapid development in suction. Between 12 and 48 h, the heat of hydration started to decrease. Also, during this period of time, the continuous formation of hydration products can be traced by a reduction of the electrical conductivity as an indication of ion depletion from the pore solution (see Fig. 18).

After 48 h of curing time, the hardening process of backfilling started to occur. No significant settlement was observed beyond this point, even under relatively high curing pressures (600 kPa). Gradual precipitation of cement hydration products (such as CH and C–S–H) refined the pore structure and caused the evolution of the engineering properties of backfill (Fall et al. 2010a). It should be stressed that the current experimental observations describe the THMC behavior of the studied material and the results may vary for other types of backfills, depending on binder content and type, curing condition (e.g., temperature), tailings properties, chemical composition of water used in the backfill preparation, etc. Furthermore, it should be expected that in the field, due to the large size of the CPB, the magnitude of the observed coupled THMC processes will be greater.

4 Summary and Conclusion

This paper has assessed and discussed the coupled THMC evolution of CPB material at early ages by means of a developed pressure cell setup. A comprehensive instrumentation program which is employed on pressure cell can successfully be used to investigate the coupled THMC processes in cemented backfill materials. The main purpose is to simulate self-weight pressure during curing time by means of a controlled pressure application rate and investigate its effects on the THMC coupled behavior of CPB in undrained conditions. The obtained results show that the physical properties of CPB, such as void ratio (and porosity), water content and bulk density, are variable with time. Also, it is noticed that the pressure application and the THM factors can significantly change the physical properties of the CPB. The evolution of these properties can influence the coupled THM factors and performance of a CPB. For example, pore refinement and porosity reduction can lead to improvement in mechanical strength and hydraulic conductivity. Also, the porosity and water content are two parameters that control the evolution of thermal conductivity in CPB materials.

The obtained results show that mechanical properties, including the UCS and modulus of elasticity, are considerably influenced by pressure application and curing time. The results indicate that there is a strong correlation between the UCS and void ratio. Suction evolution as a result of cement chemical reaction induced self-desiccation and curing stress are important mechanisms in strength development, especially in the early hours (before setting). Also, strongly H–M coupled processes govern backfill behavior, which include coupled relationships between self-desiccation and pressure application (consolidation). The stress–strain curves show that the backfill at 7 days of curing exhibits less "plastic" behavior compared to that of the 1 day cured sample. In terms of shear strength parameters, the internal friction angle obtained for all of the samples (ST and ZnT) is not a time dependent parameter, while cohesion considerably changes with time and applied curing stress. The results of the monitoring of the settlement reveal that CPB materials can undergo large volume changes after placement due to the coupled effects of pressure application induced tailings rearrangement before the setting of the CPB occurs, chemical shrinkage (self-desiccation induced consolidation) and thermal shrinkage.

The heat of cement hydration (and also curing temperature) can facilitate cement chemical reactions and therefore lead to faster strength development by increases in the rate of the suction development and decreases in the setting time. The monitoring of the pore fluid chemistry and electrical conductivity shows the mechanism of the setting time and hardening process, and contribution of chemical factors in the THMC coupled process. MIP and SEM observations support the physical mechanism of pore refinement as a result of pressure application.

A THMC behavior investigation on backfill prepared with ZnT, which contains significant chemical impurities, reveals that the chemical and mineralogical properties of tailings as well as the pore water chemistry of the tailings can significantly alter

the H–M performance, binder hydration and setting time of the CPB. The obtained results show that the THMC properties of the CPB are strongly coupled. This type of THMC behavior is fully dependent on cement hydration processes in the CPB material. Cement hydration, self-desiccation, heat development and curing stress are considered as important internal mechanisms that can affect the short-term THMC behavior of CPB structures. The developed pressure cell set-up helps to simulate a backfill close to in situ conditions and provide a better understanding of the fundamental mechanisms of THMC processes at a laboratory scale. The authors believe that the findings presented in this paper will contribute to a better understanding of the THMC coupled processes in CPB and their behaviors, and can help to design safe, economic and durable backfill structures.

Acknowledgments The authors would like to thank the Natural Sciences and Engineering Research Council of Canada (NSERC), the University of Ottawa and the industrial partners in this project.

References

Abdul-Hussain N, Fall M (2011) Unsaturated hydraulic properties of cemented tailings backfill that contains sodium silicate. Eng Geol 123(4):288–301

Abdul-Hussain N, Fall M (2012) Thermo-hydro-mechanical behaviour of sodium silicate cemented backfill in column experiments. Tunn Undergr Space Technol 29:85–93

Ahnberg H (2007) On yield stresses and the influence of curing stresses on stress paths and strength measured in triaxial testing of stabilized soils. Can Geotech J 44(1):54–66

ASTM D7263-09 (2009) Standard test methods for laboratory determination of density (unit weight) of soil specimens. ASTM International, West Conshohocken. www.astm.org

ASTM C143 (2010) Standard test method for slump of hydraulic-cement concrete. ASTM International, West Conshohocken. www.astm.org

ASTM D5084 (2010) Standard test methods for measurement of hydraulic conductivity of saturated porous materials using a flexible wall permeameter. ASTM International, West Conshohocken. www.astm.org

ASTM D3080 (2011) Standard Test method for direct shear test of soils under consolidated drained conditions. ASTM International, West Conshohocken. www.astm.org

ASTM C39 (2012) Standard test method for compressive strength of cylindrical concrete specimens. ASTM International, West Conshohocken. www.astm.org

ASTM D2216-10 (2010) Standard test methods for laboratory determination of water (moisture) content of soil and rock by mass. ASTM International, West Conshohocken. www.astm.org

Barneyback RS, Diamond S (1981) Expression and analysis of pore fluids from hardened cement pastes and mortars. Cem Concr Res 11(2):279–285

Belem T, Benzaazoua M, Bussière B, Dagenais AM (2002) Effects of settlement and drainage on strength development within mine paste backfill. In: Proceedings of tailings and mine waste'02, Fort Collins, Colorado. Balkema, Rotterdam. 27–30 Jan 2002, pp 139–148

Benzaazoua M, Fall M, Belem T (2004) A contribution to understanding the hardening process of cemented pastefill. Miner Eng 17(12):141–152

Celestin J, Fall M (2009) Thermal conductivity of cemented paste backfill material and factors affecting it. Int J Min Reclam Environ 23(4):274–290

Cihangir F, Ercikdi B, Kesimal A, Turan A, Deveci H (2012) Utilisation of alkali-activated blast furnace slag in paste backfill of high-sulphide mill tailings: effect of binder type and dosage. Miner Eng 30:33–43

Cook RA, Hover KC (1999) Mercury porosimetry of hardened cement pastes. Cem Concr Res 29:933–943

Diamond S (2004) The microstructure of cement paste and concrete—a visual primer. Cem Concr Compos 26(8):919–933

Double DD (1983) New developments in understanding the chemistry of cement hydration. Philos Trans R Soc Lond A 310(1511):53–66

Dullien FAL (1992) Porous media: fluid transport and pore structure, 2nd edn. Academic Press, New York

Ercikdi B, Cihangir F, Kesimal A, Deveci H, Alp I (2009) Utilization of industrial waste products as pozzolanic material in cemented paste backfill of high sulphide mill tailings. J Hazard Mater 168(2–3):848–856

Ercikdi B, Cihangir F, Kesimal A, Deveci H, Alp I (2010) Utilization of water-reducing admixtures in cemented paste backfill of sulphide-rich mill tailings. J Hazard Mater 179(1–3):940–946

Ercikdi B, Baki H, Izki M (2013) Effect of desliming of sulphide-rich mill tailings on the long-term strength of cemented paste backfill. J Environ Manag 115(30):5–13

Espinos RM, Franke L (2006) Influence of the age and drying process on pore structure and sorption isotherms of hardened cement paste. Cem Concr Res 36(10):1969–1984

Fall M, Benzaazoua M (2005) Modeling the effect of sulphate on strength development of paste backfill and binder mixture optimization. Cem Concr Res 35(2):301–314

Fall M, Pokharel M (2010) Coupled effect of sulphate and temperature on the strength development of cemented backfill tailings: Portland cement paste backfill. Cem Concr Compos 32(10):819–828

Fall M, Samb S (2008) Pore structure of cemented tailings materials under natural or accidental thermal loads. Mater Charact 59(5):598–605

Fall M, Samb SS (2009) Effect of high temperature on strength and microstructural properties of cemented paste backfill. Fire Saf J 44(4):642–651

Fall M, Benzaazoua M, Ouellet S (2005) Experimental characterization of the influence of tailings fineness and density on the quality of cemented paste backfill. Miner Eng 18(1):41–44

Fall M, Belem T, Samb S, Benzaazoua M (2007) Experimental characterization of the stress–strain behaviour of cemented

paste backfill in compression. J Mater Sci 42(11):3914–3992
Fall M, Benzaazoua M, Saa EG (2008) Mix proportioning of underground cemented tailings backfill. Tunn Undergr Space Technol 28(1):80–90
Fall M, Adrien D, Celestin J, Pokharel M, Toure M (2009) Saturated hydraulic conductivity of cemented paste backfill. Miner Eng 22(15):1307–1317
Fall M, Celestin J, Pokharel M, Touré M (2010a) A contribution to understanding the effects of curing temperature on the mechanical properties of mine cemented tailings backfill. Eng Geol 114(3–4):397–413
Fall M, Célestin JC, Sen HF (2010b) Potential use of polymer-pastefill as waste containment barrier materials. J Waste Manag 30:2570–2578
Farkish A, Fall M (2013) Rapid dewatering of oil sands mature fine tailings using super absorbent polymer. Miner Eng 50–51:38–47
Gawin D, Pesavento F, Schrefler BA (2007) Modelling creep and shrinkage of concrete by means of effective stresses. J Mater Struct 40(6):579–591
Ghirian A, Fall M (2013) Coupled thermo-hydro-mechanical–chemical behaviour of cemented paste backfill in column experiments. Part I: physical, hydraulic and thermal processes and characteristics. Eng Geol 164:195–207
Ghirian A, Fall M (2014) Coupled thermo-hydro-mechanical–chemical behaviour of cemented paste backfill in column experiments. Part II: mechanical, chemical and microstructural processes and characteristics. Eng Geol 170: 11–23
Godbout J (2005) Evolution des proprieties des remblais miniers cimentés en pate durant le curage. Mémoire de Maitrise, Ecole Polytechnique de Montréal, p 212
Hansen TC, Radjy FE, Sellevold EJ (1973) Cement paste and concrete. Annu Rev Mater Sci 3:233–268
Hassani F, Archibald J (1998) Mine Backfill (CD-ROM). Canadian Institute of Mine, Metallurgy and Petroleum, p 262
Helinski M (2007) Mechanics of mine backfill. PhD thesis, The University of Wstern Australia, p 259
Helinski M, Fourie AB, Fahey M (2006) Mechanics of early age cemented paste backfill. In: Proceedings of the 9th international seminar on paste and thickened tailings, Limerick, pp 313–322
Horai KI (1971) Thermal conductivity of rock-forming minerals. J Geophys Res 76(5):1278–1308
Huang S, Xia K, Qiao L (2011) Dynamic tests of cemented paste backfill: effects of strain rate, curing time, and cement content on compressive strength. J Mater Sci 46(15):5165–5170
Huynh L, Beattie DA, Fornasiero D, Ralston J (2006) Effect of polyphosphate and naphthalene sulfonate formaldehyde condensate on the rheological properties of dewatered tailings and cemented paste backfill. Miner Eng 19(1):28–36
Kesimal A, Ercikdi B, Yilmaz E (2003) The effect of desliming by sedimentation on paste backfill performance. Miner Eng 16(10):1009–1011
Kesimal A, Yilmaz E, Ercikdi B, Alp I, Deveci H (2005) Effect of properties of tailings and binder on the short and long-term strength and stability of cemented paste backfill. Mater Lett 59(28):3703–3709
Khan MI (2002) Factors affecting the thermal properties of concrete and applicability of its prediction models. Build Environ 37(7):607–614
Kim K-H, Jeon S-E, Kim J-K, Yang S (2003) An experimental study on thermal conductivity of concrete. Cem Concr Res 33(3):363–371
Klein KA, Simon D (2006) Effect of specimen composition on the strength development in cemented paste backfill. Can Geotech J 43:310–324
Landriault D (2001) Chapter 69: backfill in underground mining. In: Hustrulid WA, Bullock RL (eds) Underground mining methods: engineering fundamentals and international case studies. Society for Mining, Metallurgy and Exploration, Littleton, pp 29–48
Le Roux KA, Bawden WF, Grabinsky MW (2005) Field properties of cemented paste backfill at the Golden Giant mine. Mining Technol 114(2):65–80
Levita G, Marchetti A, Gallone G, Princigallo A, Guerrin GL (2000) Electrical properties of fluidized Portland cement mixes in the early stage of hydration. Cem Concr Res 30(6):923–930
Li L, Aubertin M (2009) Influence of water pressure on the stress state in stopes with cohesionless backfill. Geotech Geol Eng 27(1):1–11
Lothenbach B, Wieland E (2006) A thermodynamic approach to the hydration of sulphate-resisting Portland cement. Waste Manag 26(7):706–719
Lothenbach B, Winnefeld F, Alder C, Wieland E, Lunk P (2007) Effect of temperature on the pore solution, microstructure and hydration products of Portland cement pastes. Cem Concr Res 37(4):483–491
Mahlaba JS, Kearsley EP, Kruger RA, Pretorius PC (2011) Evaluation of workability and strength development of fly ash pastes prepared with industrial brines rich in and Cl^- to expand brine utilisation. Miner Eng 24(10):1077–1081
Manmohan D, Mehta PK (1981) Influence of pozzolanic slag, and chemical admixtures on PSD and permeability of hardened cement pastes. J Cem Concr Aggreg 3:63–67
Meddah SM, Tagnit-Hamou A (2011) Evaluation of rate of deformation for early-age concrete shrinkage analysis and time zero determination. J Mater Civ Eng 23(7):1076–1086
Mehta PK, Monteiro PJM (2013) Concrete: microstructure, properties, and materials, 4th edn. McGraw Hill, New York
MPS-2 Operator's Manual (2014) MPS-2 & MPS-6 dielectric water potential sensors manual. Decagon Devices, Inc., Version: December 4, 2014
Nasir O, Fall M (2008) Shear behaviour of cemented pastefill-rock interfaces. Eng Geol 101(3–4):146–153
Nasir O, Fall M (2009) Modeling the heat development in hydrating CPB structures. Comput Geotech 36(7):1207–1218
Nasir O, Fall M (2010) Coupling binder hydration, temperature and compressive strength development of underground cemented paste backfill at early ages. Tunn Undergr Space Technol 25(1):9–20
Orejarena L, Fall M (2008) Mechanical response of a mine composite material to extreme heat. Bull Eng Geol Environ 67(3):387–396
Orejarena L, Fall M (2010) The use of artificial neural network to predict the effect of sulphate on the strength of cemented paste backfill. Bull Eng Geol Environ 69(4):659–670

Orejarena L, Fall M (2011) Artificial neural network based modeling of the coupled effect of sulphate and temperature on the strength of cemented paste backfill. Can J Civ Eng 38(1):100–109

Pacheco-Torgal F, Castro-Gomes J, Jalali S (2007) Investigations about the effect of aggregates on strength and microstructure of geopolymeric mine waste mud binders. Cem Concr Res 37(6):933–941

Pokharel M, Fall M (2011) Coupled thermo-chemical effects on the strength development on Slag-Paste backfill materials. ASCE J Mater Civil Eng 23(5):511–525

Rankine RM, Rankine KJ, Sivakugan N, Karunasena W, Bloss ML (2001) Geotechnical characterisation and stability analysis of BHP Cannington paste. II. In: Proceedings of the 15th international conference on soil mechanics and geotechnical engineering, pp 1241–1244

Ritcey GM (2005) Tailings management in gold plants. Hydrometallurgy 78(1–2):3–20

Swaddiwudhipong S, Chen D, Zhang MH (2002) Simulation of the exothermic process of Portland cement. Adv Cem Res 14(2):61–69

Taylor HFW (1997) Cement Chemistry, 2nd edn. Thomas Telford Publishing, London

Thompson BD, Grabinsky MW, Bawden WF (2009) In-situ measurements of cemented paste backfill in long-hole stope. In: Proceedings of the 3rd CANUS rock mechanics symposium, Toronto

Thottarath S (2010) Electromagnetic characterization of cemented paste backfill in the field and laboratory. Master thesis, p 105

Tzouvalas G, Dermatas N, Tsimas S (2004) Alternative calcium sulfate-bearing materials as cement retarders: part I. Anhydrite. Cem Concr Res 34(11):2113–2118

Wu D, Fall M, Cai S-J (2012) Coupled modeling of temperature distribution and evolution in cemented tailings backfill structures that contains mineral admixtures. J Geotech Geol. doi:10.1007/s10706-012-9518-1

Wu D, Fall M, Cai S-J (2013) Coupling temperature, cement hydration and rheological behaviour of cemented paste backfill structures. Miner Eng 42:76–87

Yilmaz E, Kesimal A, Deveci H, Ercikdi B (2003) The factors affecting the performance of paste backfill: physical, chemical and mineralogical characterization. First engineering sciences congress for young researcher (MBGAK'03), Istanbul

Yilmaz E, Kesimal A, Ercidi B (2004) Strength development of paste backfill simples at Long term using different binders. In: Proceedings of 8th symposium MineFill04, China, pp 281–285

Yilmaz E, Benzaazoua M, Belem T, Bussiere B (2009) Effect of curing under pressure on compressive strength development of cemented paste backfill. Miner Eng 22(9–10): 772–785

Yilmaz E, Belem T, Benzaazoua M (2014) Effects of curing and stress conditions on hydromechanical, geotechnical and geochemical of cemented paste backfills. Eng Geol 168: 23–37

Yin S, Wu A, Hu K, Wang Y, Zhang Y (2012) The effect of solid components on the rheological and mechanical properties of cemented paste backfill. Miner Eng 35:61–66

Zhou Q, Beaudoin JJ (2003) Effect of applied hydrostatic stress on the hydration of Portland cement and C3S. Adv Cem Res 15(1):9–16